JOURNAL OF PETROLOGY | VOLUME 48 | NUMBER 10 | PAGES 1999–2031 | 2007 | doi:10.1093/petrology/egm048

Wet and Dry Basalt Magma Evolution at Torishima Volcano, Izu–Bonin Arc, Japan: the Possible Role of Phengite in the Downgoing Slab

Y. TAMURA[1]*, K. TANI[1], Q. CHANG[1], H. SHUKUNO[1], H. KAWABATA[1], O. ISHIZUKA[2] AND R. S. FISKE[3]

[1]INSTITUTE FOR RESEARCH ON EARTH EVOLUTION (IFREE), JAPAN AGENCY FOR MARINE–EARTH SCIENCE AND TECHNOLOGY (JAMSTEC), YOKOSUKA 237-0061, JAPAN

[2]INSTITUTE OF GEOSCIENCE, GEOLOGICAL SURVEY OF JAPAN/AIST, TSUKUBA 305-8567, JAPAN

[3]SMITHSONIAN INSTITUTION, WASHINGTON, DC 20560, USA

RECEIVED OCTOBER 18, 2006; ACCEPTED JULY 27, 2007
ADVANCE ACCESS PUBLICATION AUGUST 27, 2007

The arc-front volcanoes of Sumisu (31·5°N, 140°E) and Torishima (30·5°N, 140·3°E) in the central Izu–Bonin arc are similar in size and rise as relatively isolated edifices from the seafloor. Together they provide valuable along-arc information about magma generation processes. The volcanoes have erupted low-K basalts originating from both wet and dry parental basaltic magmas (low-Zr basalts and high-Zr basalts, respectively). Based on models involving fluid-immobile incompatible element ratios (La/Sm), the parental basalts appear to result from different degrees of partial melting of the same source mantle (~20% and ~10% for wet and dry basalt magmas, respectively). Assuming that the wet basalts contain greater abundances of slab-derived components than their dry counterparts, geochemical comparison of these two basalt types permits the identification of the specific elements involved in fluid transport from the subducting slab. Using an extensive set of new geochemical data from Torishima, where the top of the downgoing slab is about 100 km deep, we find that Cs, Pb, and Sr are variably enriched in the low-Zr basalts, which cannot be accounted for by fractional crystallization or by differences in the degree of mantle melting. These elements are interpreted to be selectively concentrated in slab-derived metasomatic fluids. Variations in K, high field strength element and rare earth element concentrations are readily explained by variations in the degree of melting between the low- and high-Zr basalts; these elements are not contained in the slab-derived fluids. Rb and Ba exhibit variable behaviour in the low-Zr basalts, ranging from immobile, similar to K, to mildly enriched in some low-Zr basalts. We suggest that the K-rich mica, phengite, plays an important role in determining the composition of fluids released from the downgoing slab. In arc-front settings, where slab depth is ≤100 km, phengite is stable, and the fluids released from the slab contain little K. In back-arc settings, however, where the slab is at 100–140 km depth, phengite is unstable, and K-rich fluids are released. We conclude that cross-arc variations in the K content of arc basalts are probably related to differing compositions of released fluids or melts rather than the widely held view that such variations are controlled by the degree of partial melting.

KEY WORDS: *arc volcano; degrees of melting; mantle wedge; water; wet and dry basalts*

INTRODUCTION

The Izu–Bonin volcanic arc is an excellent example of an intra-oceanic convergent margin system (Fig. 1). The geochemistry of volcanic front magmatism at Sumisu volcano is well known from studies of Sumisu island, as well as dredging and ROV or submersible dives in the adjacent Sumisu submarine caldera (Tamura *et al.*, 2005; Shukuno *et al.*, 2006; Tani *et al.*, 2007). Evidence for involvement of both dry and wet basalts as parental liquids in the genesis of Sumisu volcano was presented by Tamura *et al.* (2005). The chief aims of this study are: (1) to interpret new data from the nearby arc-front volcano Torishima; (2) to consider the petrogenesis of the two types of basalt to gain

*Corresponding author. Telephone: +81-46-867-9761. Fax: +81-46-867-9625. E-mail: tamuray@jamstec.go.jp

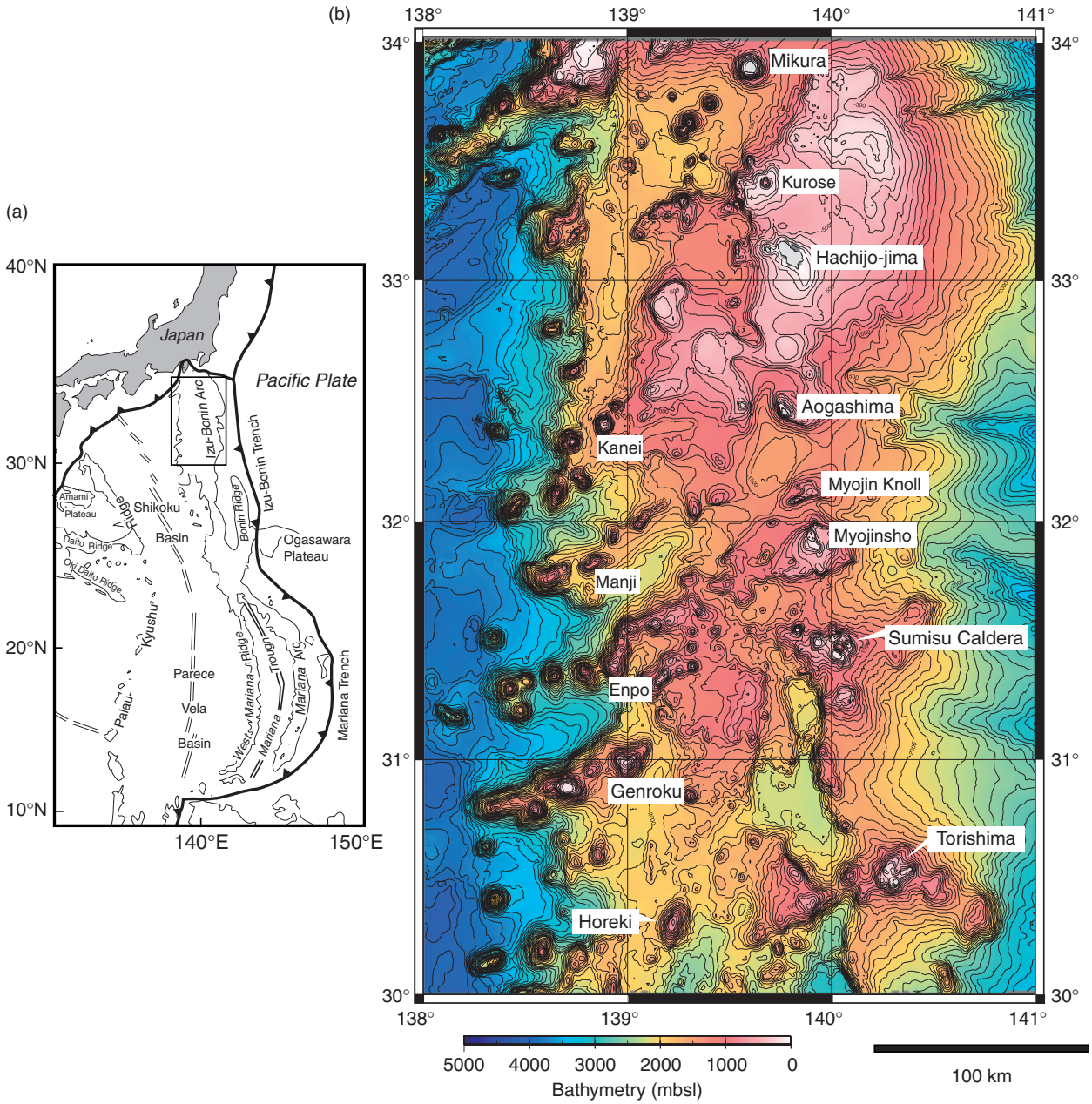

Fig. 1. (a) Map of the Izu–Bonin Mariana system (after Taylor, 1992). (b) Seafloor bathymetry of the northern Izu–Bonin arc. The Quaternary arc-front volcanoes (Mikura, Kurose, Hachijo-jima, Aogashima, Myojin Knoll, Myojinsho, Sumisu, Torishima) and Plio-Miocene seamount chains in the rear arc (Kanei, Manji, Enpo, Genroku, Horeki) are shown. The summits of some frontal volcanoes have grown above sea level to form the Izu–Ogasawara (Bonin) islands.

an insight into the nature of the slab-derived component; (3) to evaluate the role of phengite in the subducting slab. Torishima lies 110 km SSE of Sumisu, and the two volcanoes rise as relatively isolated edifices of similar size from the arc-front ridge (Fig. 1). A combined study of these two volcanic systems can provide a relatively simple 2-D along-arc perspective of magma genesis in an environment little contaminated by complex pre-volcanic histories.

Elliott *et al.* (1997) documented island-to-island geochemical variations among the Mariana arc volcanoes to the south. Their two-component model suggests that the main differences in the composition of the lavas erupted from different islands of the Marianas are due to the addition of variable amounts of melted sediment to their sources. Signatures of aqueous fluid addition are inversely correlated with indices of sediment melt

contribution, which is likely only if the aqueous fluid flux across the entire arc is fairly constant. Our study of Torishima and that of Sumisu by Tamura *et al.* (2005) focuses on variations within and between these two volcanoes, based on samples obtained from both the subaerial and submarine parts.

From this study, we conclude that the arc-front volcano Torishima contains basalts originating from both wet and dry parental basalt magmas, a situation similar to that found at Sumisu. The extensive dataset for Torishima makes it possible to compare these two types of basalt in detail. Based on the assumption that wet basalts contain more slab-derived fluids than dry basalts, it is shown that Cs, Pb and Sr are selectively concentrated in the slab-derived fluids below this frontal volcano, whereas potassium, high field strength elements (HFSE) and rare earth elements (REE) are not. The behaviour of Rb and Ba is intermediate between that of Th and K and Cs and Sr, suggesting that they are mildly immobile in the aqueous fluid. We suggest that phengite (a potassium-rich mica) plays a role in temporarily immobilizing K, partitioning the large ion lithophile elements (LILE) into fluids and causing fractionation of LILE (Cs/Rb and Cs/Ba) below the volcanic front (Schmidt, 1996; Domanik & Holloway, 1996; Melzer & Wunder, 2000; Green & Adam, 2003).

Transverse geochemical variations across the Izu–Bonin arc and other volcanic arcs have been discussed extensively in the literature (Kuno, 1960, 1966; for summary, see Gill, 1981, p. 209; Tatsumi & Eggins, 1995; Hochstaedter *et al.*, 2000, 2001). Based on data compiled from the Izu–Bonin arc volcanoes, we suggest here that such cross-arc variations need not be the result of greater degrees of partial melting beneath frontal regions (e.g. Sakuyama & Nesbitt, 1986; Kushiro, 1994) but may instead be related to the transient stability of phengite in the downgoing slab.

ANALYTICAL METHODS

After initial splitting and jaw crushing, all samples were pulverized in an agate ball mill. Major and trace elements were determined by X-ray fluorescence (XRF) at IFREE, JAMSTEC. Trace elements were analyzed on pressed powder discs, and major elements were determined on fused glass discs. A mixture of ~0·4 g of each powdered sample and 4 g of anhydrous lithium tetraborate ($Li_2B_4O_7$) was used; no matrix correction was applied because of the high dilution involved. The REE and some trace elements were determined by inductively coupled plasma mass spectrometry (ICP-MS) using a VG Elemental® PQ3 instrument enhanced with a chicane lens system, following the procedures described by Chang *et al.* (2003). Accurately weighed 100 mg aliquots of powdered samples were digested in screw-cap PFA vials with mixed acids (0·65 ml $HClO_4$ and 2 ml HF) on a hot plate at 130–140°C for 3 days. After drying, 1 ml $HClO_4$ was added, the vials were heated at 160°C overnight, and they were then opened to evaporate the solutions at a gradually increased temperature of up to 190°C to drive off excess HF and convert the fluoride into chlorides. The residues were taken into 2 ml of 6 mol/l HNO_3, moderately heated and then evaporated at 120°C to incipient dryness. The final dissolution was performed with 10 ml of 2% HNO_3. Prior to analysis, In and Bi were added to aliquots of sample solutions as internal standards to correct signal drifts during measurements. Typical dilution factors from this preparation procedure were about 7500 for the samples analyzed. The ICP-MS system was optimized to a sensitivity of *c.* 120 000 c.p.s./ppb and 100 000 c.p.s./ppb for ^{115}In and ^{209}Bi, respectively, and Ce oxide formation of less than 0·5%. Measured Eu and Gd concentrations were corrected for oxide and hydroxide interferences. The analytical results of repeated analyses of well-established reference standards (JB-2 and BHVO-1) agreed very well with recommended values, proving that the REE and trace element determinations were performed at high accuracy and reproducibility. Representative major and trace element data for basaltic rocks from Torishima volcano are reported in Table 1. The entire XRF dataset and modal mineralogy of volcanic rocks from Torishima volcano, ranging from basalt to rhyolite, are available as an Electronic Appendix, which may be downloaded from http://www.petrology.oxfordjournals.org/. All major element data have been normalized to 100% on a volatile-free basis, with total iron calculated as FeO.

Electron microprobe analyses were carried out using the JAMSTEC JEOL JXA-8900 Superprobe equipped with five wavelength-dispersive spectrometers (WDS). Olivine analyses were made with a counting time of 100 s, an accelerating voltage of 20 kV, a beam current of 25 nA and a probe diameter of 5 μm to ensure reliable Ni values. Pyroxene and plagioclase analyses were made with a counting time of 20 s, an accelerating voltage of 15 kV and a beam current of 15 nA. Representative mineral compositions in basalts and basaltic andesites from Torishima volcano are given in Table 2.

TORISHIMA VOLCANO

The bathymetric map shows that the main edifice of Torishima volcano rises from an ocean depth of ~1000 m (Fig. 2). The volcano is about 20 km in diameter, and Torishima island lies along the south rim of a submarine caldera. The surrounding sea floor was dredged during the December 2002 cruise of the R.V. *Kairei* (KR02-16) (Fig. 2); Torishima island was studied and sampled during a 2 week field expedition in 2003. Fifty-six dredge samples and 141 samples from the island were analyzed

Table 1: Representative major and trace element data, and modal analyses for basaltic rocks from Torishima volcano

Unit:	OP	OP	OP	OP	OP	OP	OP	OP	OP	OP	Dredge	Dredge	YP	Dredge	YP	1939	1939	YP	YP	Ref.	σ	Compiled
Sample:	33	35.5	35	99	64	69	142	85	140	89	D9-R10	D19-R12	11	D15-R04	7	24	37	26	1	standard		standard
Rock:	L	L	L	L	L	L	L	L	L	L	H	H	H	H	H	H	H	H	H	average*		value
	lava	boulder	boulder	lava	dike	dike	boulder	dike	dike	dike	lava	lava	lava	lava	lava	lava	lava	lava	boulder			
wt %																						
SiO_2	48·80	48·59	48·87	49·12	48·92	48·96	48·81	48·72	48·84	49·20	51·72	51·09	51·51	50·75	51·15	54·66	54·49	51·15	51·80	50·50	0·011	50·96
TiO_2	0·56	0·56	0·60	0·63	0·58	0·58	0·63	0·61	0·68	0·59	0·62	0·61	0·69	0·66	0·58	0·79	0·78	0·61	0·65	1·46	0·002	1·44
Al_2O_3	18·08	18·23	18·26	18·65	19·40	19·51	19·94	20·09	19·73	20·30	16·75	17·64	17·39	18·51	19·73	17·02	17·16	20·53	20·59	17·33	0·011	17·20
Fe_2O_3	11·15	11·10	11·37	11·50	10·78	10·78	11·08	10·92	11·48	10·87	11·31	11·21	11·53	11·05	9·94	11·66	11·63	9·84	9·92	11·88	0·002	11·82
MnO	0·18	0·18	0·18	0·18	0·17	0·17	0·17	0·17	0·18	0·17	0·19	0·18	0·19	0·18	0·16	0·20	0·20	0·15	0·15	0·17	0·000	0·18
MgO	7·65	7·61	7·06	6·11	5·96	5·94	5·55	5·40	5·37	5·15	6·68	6·21	5·90	5·31	4·94	4·08	4·04	4·00	3·38	5·15	0·019	5·19
CaO	13·63	13·55	13·50	13·45	13·71	13·74	13·64	13·61	13·45	13·06	11·26	11·73	11·71	12·13	12·33	9·62	9·50	12·06	11·68	9·88	0·003	9·79
Na_2O	1·29	1·27	1·33	1·41	1·36	1·36	1·44	1·47	1·39	1·56	1·87	1·83	1·90	1·91	1·78	2·66	2·61	1·91	2·22	2·74	0·019	2·73
K_2O	0·09	0·09	0·10	0·11	0·11	0·10	0·09	0·07	0·07	0·12	0·22	0·22	0·24	0·15	0·21	0·30	0·30	0·23	0·29	0·76	0·001	0·78
P_2O_5	0·05	0·05	0·05	0·06	0·05	0·05	0·06	0·06	0·06	0·06	0·07	0·08	0·08	0·08	0·08	0·18	0·17	0·08	0·08	0·30	0·001	0·29
Total	101·48	101·22	101·31	101·21	101·04	101·19	101·40	101·11	101·24	101·08	100·68	100·79	101·14	100·72	100·90	101·16	100·87	100·56	100·75	100·17		100·38
Trace elements (ppm) by XRF																						
Ba	31·6	44·4	39·9	32·7	29·2	36·3	44·1	48·2	40·5	56·9	60·4	49·4	72·7	57·6	59·7	75·7	84·2	57·2	73·0	503	11·5	493
Ni	30·6	34·5	29·7	22·7	23·1	25·5	21·3	22·3	23·9	18·9	38·7	28·2	22·4	22·8	19·2	10·5	13·7	12·8	11·9	122	1·01	133
Cu	162·5	177·5	165·8	200·9	187·4	178·6	213·8	248·7	236·8	179·7	105·9	104·9	163·7	144·4	78·5	165·0	145·2	69·0	132·0	56·7	0·941	55·1
Zn	65·2	64·4	66·6	66·4	64·9	65·8	66·4	65·3	69·9	68·6	79·4	82·6	74·9	77·8	64·2	94·8	91·9	65·2	65·2	82·8	0·826	85·2
Pb	1·7							1·7		1·7	2·0	1·9	1·6			3·1	3·1	2·6	2·9	7·60	0·545	7·10
Th						0·6										1·1				10·1	0·448	9·30
Rb	1·5	1·3	1·6	1·8	1·8	1·6	1·6	0·8	0·9	2·0	2·9	3·1	3·2	1·5	2·4	3·9	4·0	2·7	3·6	41·0	0·127	41·3
Sr	157·1	159·3	161·3	171·1	167·9	169·0	178·1	175·3	179·0	178·5	166·8	171·1	167·5	166·6	185·3	183·7	184·7	194·7	199·9	460	1·13	444
Y	9·6	9·8	10·1	11·0	10·3	10·1	10·3	10·6	10·8	10·9	14·5	13·5	16·1	14·9	13·1	20·5	19·4	14·9	16·5	20·9	0·272	24·3
Zr	14·6	14·6	16·0	16·6	15·7	15·8	15·2	16·0	16·2	18·0	27·4	23·2	30·8	24·2	26·4	36·1	36·6	28·5	32·3	134	0·600	141
Nb		0·4	0·5			0·6					0·2	0·5	0·5	0·4	0·6		0·7	0·4	0·4	33·1	0·220	33·3
S								849·5	43·4		3·2				120·6		577·7					
Trace elements (ppm) by ICP-MS																						
Sc	45·7	43·7	45·1	46·0	41·0	40·8	40·4	39·3	40·2	38·1	50·5	47·1	43·2	50·9	36·2	37·7	37·0	32·4	30·3	53·2		53·5
Y	9·6	9·6	10·3	10·9	10·1	10·1	10·3	10·3	11·0	11·2	15·8	14·2	16·2	16·0	13·3	20·9	19·1	14·5	16·2	23·4	1·1	24·9
Cs	0·114	0·106	0·121	0·139	0·141	0·136	0·119	0·095	0·094	0·135	0·273	0·263	0·280	0·118	0·133	0·327	0·317	0·172	0·085	0·798	0·018	0·85
La	0·694	0·700	0·738	0·857	0·730	0·727	0·765	0·760	0·835	0·940	1·45	1·33	1·65	1·20	1·18	2·04	2·01	1·49	1·71	2·25	0·05	2·35

JOURNAL OF PETROLOGY | VOLUME 48 | NUMBER 10 | OCTOBER 2007

Unit:	OP	OP	OP	OP	OP	OP	OP	OP	OP	OP	Dredge	Dredge	YP	Dredge	YP	1939	1939	YP	YP	Ref.	σ	Compiled
Sample:	33	35.5	35	99	64	69	142	85	140	89	D9-R10	D19-R12	11	D15-R04	7	24	37	26	1	standard		standard
Rock:	L	L	L	L	L	L	L	L	L	L	H	H	H	H	H	H	H	H	H	average*		value
	lava	boulder	boulder	lava	dike	dike	boulder	dike	dike	dike	lava	lava	lava	lava	lava	lava	lava	lava	boulder			
Ce	2·10	2·12	2·26	2·52	2·22	2·22	2·28	2·29	2·47	2·75	4·05	3·73	4·67	3·53	3·45	5·91	5·81	4·32	4·86	6·58	0·10	6·76
Pr	0·395	0·398	0·426	0·467	0·422	0·421	0·430	0·437	0·468	0·508	0·733	0·669	0·846	0·664	0·628	1·080	1·060	0·772	0·878	1·14	0·02	1·01
Nd	2·37	2·38	2·55	2·81	2·52	2·51	2·59	2·60	2·79	2·97	4·14	3·78	4·75	3·87	3·57	6·18	5·93	4·33	4·82	6·39	0·15	6·63
Sm	0·97	0·96	1·03	1·10	1·01	1·02	1·03	1·04	1·08	1·14	1·48	1·38	1·75	1·46	1·35	2·28	2·13	1·58	1·75	2·30	0·07	2·31
Eu	0·420	0·427	0·446	0·475	0·443	0·442	0·452	0·456	0·476	0·488	0·576	0·552	0·660	0·595	0·571	0·864	0·831	0·607	0·664	0·836	0·021	0·86
Gd	1·45	1·46	1·57	1·64	1·53	1·51	1·54	1·57	1·65	1·68	2·13	1·94	2·51	2·17	1·98	3·23	2·97	2·23	2·48	3·24	0·09	3·28
Tb	0·268	0·270	0·285	0·302	0·281	0·279	0·283	0·285	0·303	0·309	0·379	0·345	0·457	0·395	0·365	0·583	0·532	0·404	0·441	0·588	0·013	0·6
Dy	1·87	1·89	1·99	2·12	1·96	1·98	1·97	2·02	2·12	2·17	2·57	2·38	3·13	2·66	2·50	3·89	3·56	2·73	3·01	4·02	0·08	3·73
Ho	0·411	0·416	0·438	0·461	0·430	0·430	0·431	0·437	0·459	0·470	0·568	0·522	0·693	0·587	0·557	0·864	0·795	0·607	0·666	0·876	0·021	0·75
Er	1·24	1·25	1·32	1·41	1·30	1·31	1·32	1·33	1·40	1·44	1·71	1·55	2·04	1·77	1·68	2·58	2·40	1·81	2·00	2·62	0·06	2·6
Tm	0·179	0·179	0·190	0·204	0·188	0·189	0·191	0·193	0·203	0·208	0·254	0·230	0·302	0·263	0·251	0·381	0·351	0·271	0·296	0·382	0·008	0·41
Yb	1·20	1·22	1·30	1·35	1·27	1·26	1·27	1·30	1·35	1·40	1·67	1·52	1·97	1·69	1·67	2·51	2·35	1·79	1·98	2·56	0·05	2·62
Lu	0·183	0·182	0·195	0·208	0·194	0·194	0·192	0·196	0·207	0·215	0·261	0·241	0·311	0·264	0·259	0·391	0·365	0·277	0·302	0·387	0·008	0·4
Tl	0·008	0·006	0·006	0·009	0·011	0·010	0·009	0·007	0·010	0·010	0·031	0·029	0·019	0·009	0·014	0·038	0·041	0·027	0·016	0·038	0·002	0·042
Pb	0·878	0·866	0·939	0·930	0·928	0·903	0·71	0·980	1·06	1·012	1·52	1·53	1·71	1·25	1·30	2·53	1·96	2·89	2·24	5·48	0·079	5·36
Th	0·060	0·056	0·060	0·073	0·059	0·057	0·065	0·063	0·072	0·084	0·129	0·104	0·162	0·079	0·137	0·172	0·174	0·151	0·170	0·282	0·006	0·35
U	0·043	0·048	0·056	0·057	0·047	0·045	0·046	0·050	0·057	0·065	0·099	0·084	0·135	0·071	0·109	0·147	0·143	0·130	0·145	0·163	0·005	0·18
Rb	1·45	1·40	1·55	1·76	1·56	1·54	1·39	0·96	1·06	1·82	2·84	2·70	3·17	1·62	2·35	3·59	3·53	2·58	3·12	6·91	0·12	7·37
Sr	164	164	167	176	174	175	183	181	184	187	163	169	159	164	178	177	176	188	190·4	182·6	3·1	178
Ba	27·1	27·1	28·8	32·0	30·3	30·1	29·2	29·5	27·8	35·5	53·5	42·1	60·8	45·4	54·0	72·8	73·3	54·4	66·9	215·5	2·4	222
Modal analyses (vol.%) based on 4000–5000 points counts																						
olivine	4·4	5·0	4·9	3·9	2·4	1·9	2·2	2·2	2·3	2·9	1·4	2·1	0·6	2·2	2·1	–	0·3	0·3	–			
cpx	8·7	8·8	10·6	4·3	1·9	2·0	1·9	0·0	1·2	1·7	4·6	1·5	11·7	0·8	3·9	0·8	0·8	–	0·8			
opx	–	–	–	–	–	–	–	–	–	–	trace	–	0·8	–	–	–	0·1	–	0·7			
opaque	–	–	–	–	–	–	–	–	–	–	–	–	–	–	–	–	–	–	1·0			
pl	35·4	34·0	32·7	29·3	32·9	34·2	31·7	37·8	32·4	32·2	5·2	14·2	36·1	24·4	32·4	20·5	16·8	36·8	37·9			
GM	51·4	52·2	51·8	62·6	62·8	62·0	64·3	60·0	64·1	63·2	88·8	82·2	50·9	72·6	61·6	78·6	82·0	63·0	59·7			
Total	100·0	100·0	100·0	100·0	100·0	100·0	100·0	100·0	100·0	100·0	100·0	100·0	100·0	100·0	100·0	100·0	100·0	100·0	100·0			

OP, Older prehistoric units; Dredge, samples collected during JAMSTEC cruise in December 2002 (KR02-16); YP, younger prehistoric units; 1939, products of 1939 eruption; H, high-Zr basalt; L, low-Zr basalt; cpx, clinopyroxene; opx, orthopyroxene; pl, plagioclase; GM, groundmass. The entire dataset of XRF results and modal analyses for rocks from Torishima volcano, ranging from basalt to rhyolite, is available as an Electronic Appendix. The localities for samples obtained by dredge hauls and field survey are indicated in Figs 2 and 3, respectively. Compiled standard values from Imai *et al*. (1995).

*For major elements, reference standard was JB-3 ($n = 10$); for trace elements determined by XRF, reference standard was JB-1 ($n = 10$); for trace elements determined by ICP-MS, reference standard was JB-2 ($n = 5$).

Table 2: Representative mineral compositions in low-Zr and high Zr basalts and basaltic andesites

	Olivine						Olivine				Olivine			
	Low-Zr	29					Low-Zr	32			Low-Zr	35		
	4-c	4-r	9-c	9-r	16-c	16-r	3-ol1-c	3-ol1-r	3-ol2-c	3-ol2-r	4-ol1-c	4-ol1-r	15-ol-c	15-ol-r
wt %														
SiO_2	39·67	38·87	40·12	38·77	39·12	38·76	40·49	39·82	40·56	39·00	40·08	39·33	39·78	39·84
TiO_2	0·02	0·00	0·02	0·00	0·00	0·01	0·02	0·00	0·02	0·00	0·02	0·00	0·00	0·00
Al_2O_3	0·02	0·02	0·01	0·01	0·02	0·02	0·03	0·00	0·03	0·02	0·02	0·02	0·02	0·02
FeO	18·07	23·80	15·49	23·56	16·95	23·40	12·77	16·44	12·79	20·13	15·12	17·90	15·11	18·06
MnO	0·26	0·31	0·21	0·31	0·23	0·29	0·20	0·25	0·20	0·32	0·19	0·22	0·20	0·24
MgO	42·45	37·65	44·94	38·39	43·44	38·74	46·91	44·32	47·06	40·96	45·42	42·27	45·07	42·84
CaO	0·20	0·19	0·18	0·18	0·19	0·18	0·20	0·18	0·21	0·20	0·20	0·19	0·19	0·18
NiO	0·048	0·037	0·058	0·044	0·049	0·048	0·122	0·084	0·097	0·051	0·078	0·062	0·059	0·068
Total	100·73	100·87	101·03	101·24	99·99	101·44	100·74	101·09	100·96	100·69	101·12	99·99	100·41	101·24
Cations (O = 4)														
Si	1·003	1·008	0·999	1·001	0·993	0·998	0·999	0·996	0·998	0·997	0·996	1·001	0·996	1·001
Ti	0·001	0·000	0·000	0·000	0·000	0·000	0·000	0·000	0·000	0·000	0·000	0·000	0·000	0·000
Al	0·000	0·001	0·000	0·000	0·001	0·001	0·001	0·000	0·001	0·001	0·001	0·001	0·000	0·000
Fe	0·382	0·516	0·323	0·509	0·360	0·504	0·263	0·344	0·263	0·430	0·314	0·381	0·316	0·380
Mn	0·006	0·007	0·004	0·007	0·005	0·006	0·004	0·005	0·004	0·007	0·004	0·005	0·004	0·005
Mg	1·599	1·455	1·668	1·477	1·643	1·487	1·725	1·652	1·727	1·561	1·682	1·604	1·682	1·606
Ca	0·005	0·005	0·005	0·005	0·005	0·005	0·005	0·005	0·006	0·006	0·005	0·005	0·005	0·005
Ni	0·001	0·001	0·001	0·001	0·001	0·001	0·002	0·002	0·002	0·001	0·002	0·001	0·001	0·001
Total	2·997	2·992	3·001	2·999	3·007	3·002	3·000	3·004	3·001	3·003	3·004	2·998	3·004	2·998
mol%														
Fo	80·7	73·8	83·8	74·4	82·0	74·7	86·3	82·8	86·8	78·4	84·3	80·8	84·2	80·9

	Olivine				Olivine				Olivine					
	High-Zr	D9-R10			High-Zr	D15-R4			High-Zr	D19-R12				
	15-1-c	15-1-r	19-1-c	19-1-r	4-4-c	4-4-r	7-2-c	7-2-r	28-c	28-r	1-1-c	1-1-r	3-1-c	3-1-r
wt %														
SiO_2	40·39	40·18	40·69	40·65	39·26	38·70	39·28	38·45	40·11	39·08	39·63	39·22	39·83	39·39
TiO_2	0·00	0·02	0·00	0·00	0·02	0·00	0·03	0·01	0·00	0·00	0·00	0·00	0·01	0·01
Al_2O_3	0·00	0·00	0·02	0·01	0·02	0·00	0·01	0·01	0·00	0·01	0·02	0·02	0·01	0·02
FeO	14·07	17·49	13·89	13·31	21·90	25·57	21·67	25·87	16·86	19·00	18·72	21·24	18·45	19·73
MnO	0·23	0·27	0·23	0·23	0·36	0·44	0·37	0·44	0·29	0·32	0·30	0·36	0·29	0·33
MgO	45·64	44·04	46·33	46·12	40·02	36·70	39·31	36·47	43·91	41·23	42·02	40·44	42·64	41·16
CaO	0·21	0·18	0·21	0·23	0·20	0·19	0·20	0·20	0·18	0·18	0·17	0·21	0·16	0·20
NiO	0·09	0·08	0·10	0·10	0·04	0·04	0·05	0·04	0·07	0·05	0·07	0·04	0·08	0·05
Total	100·61	102·25	101·47	100·65	101·82	101·64	100·92	101·48	101·42	99·88	100·92	101·52	101·48	100·88
Cations (O = 4)														
Si	1·003	0·997	1·001	1·005	1·000	1·004	1·008	1·002	1·001	1·002	1·003	0·999	1·001	1·002
Ti	0·000	0·000	0·000	0·000	0·000	0·000	0·001	0·000	0·000	0·000	0·000	0·000	0·000	0·000
Al	0·000	0·000	0·001	0·000	0·000	0·000	0·000	0·000	0·000	0·000	0·001	0·000	0·000	0·001
Fe	0·292	0·363	0·286	0·275	0·466	0·555	0·465	0·564	0·352	0·407	0·396	0·452	0·388	0·420
Mn	0·005	0·006	0·005	0·005	0·008	0·010	0·008	0·010	0·006	0·007	0·006	0·008	0·006	0·007
Mg	1·690	1·630	1·699	1·700	1·519	1·420	1·504	1·416	1·634	1·576	1·585	1·535	1·597	1·561
Ca	0·006	0·005	0·005	0·006	0·005	0·005	0·006	0·005	0·005	0·005	0·005	0·006	0·004	0·005
Ni	0·002	0·002	0·002	0·002	0·001	0·001	0·001	0·001	0·001	0·001	0·001	0·001	0·002	0·001
Total	2·997	3·002	2·999	2·994	3·000	2·996	2·992	2·998	2·999	2·998	2·997	3·001	2·999	2·997
mol%														
Fo	85·3	81·8	85·6	86·1	76·5	71·9	76·4	71·5	82·3	79·5	80·0	77·2	80·5	78·8

(continued)

Table 2: Continued

	Clinopyroxene						Clinopyroxene				Clinopyroxene			
	Low-Zr	29					Low-Zr	32			Low-Zr	35		
	4-c	4-r	9-c	9-r	65-c	65-r	22-c	22-r	51-c	51l-r	10-c	10-r	8-c	8-r
wt %														
SiO_2	53·71	52·65	52·84	51·81	53·44	53·07	52·11	52·76	52·55	52·82	52·51	51·37	52·48	52·08
TiO_2	0·18	0·42	0·21	0·44	0·18	0·23	0·28	0·29	0·24	0·33	0·19	0·37	0·28	0·32
Al_2O_3	2·55	2·23	3·74	2·22	2·82	2·21	3·36	1·92	2·87	2·60	3·16	3·21	3·31	4·26
Cr_2O_3	0·00	0·00	0·16	0·00	0·13	0·06	0·12	0·06	0·21	0·08	0·11	0·05	0·12	0·05
FeO	6·70	12·25	4·61	13·99	4·21	7·98	6·12	13·41	4·32	7·36	5·31	8·63	6·51	11·14
MnO	0·21	0·33	0·10	0·32	0·10	0·21	0·19	0·42	0·10	0·24	0·10	0·21	0·19	0·32
MgO	16·80	16·87	16·16	15·38	17·03	16·88	15·90	18·93	15·98	16·08	15·66	15·69	16·07	15·49
CaO	21·33	15·98	23·08	15·75	23·34	19·77	21·22	11·95	22·74	20·39	22·04	19·52	20·95	15·97
Na_2O	0·15	0·14	0·09	0·21	0·12	0·16	0·17	0·10	0·11	0·16	0·06	0·14	0·17	0·21
Total	101·62	100·87	100·99	100·11	101·38	100·60	99·45	99·86	99·14	100·06	99·14	99·22	100·07	99·87
Cations (O = 6)														
Si	1·941	1·940	1·914	1·941	1·927	1·944	1·923	1·952	1·937	1·942	1·938	1·916	1·925	1·926
Ti	0·005	0·012	0·006	0·012	0·005	0·006	0·008	0·008	0·007	0·009	0·005	0·010	0·008	0·009
Al	0·108	0·097	0·160	0·098	0·120	0·095	0·146	0·084	0·125	0·113	0·137	0·141	0·143	0·186
Cr	0·000	0·000	0·005	0·000	0·004	0·002	0·003	0·002	0·006	0·002	0·003	0·001	0·003	0·001
Fe	0·203	0·378	0·140	0·438	0·127	0·244	0·189	0·415	0·133	0·226	0·164	0·269	0·200	0·344
Mn	0·006	0·010	0·003	0·010	0·003	0·007	0·006	0·013	0·003	0·007	0·003	0·007	0·006	0·010
Mg	0·905	0·927	0·873	0·859	0·916	0·922	0·875	1·044	0·878	0·881	0·862	0·872	0·879	0·854
Ca	0·826	0·631	0·896	0·632	0·902	0·776	0·839	0·474	0·898	0·803	0·872	0·780	0·823	0·633
Na	0·010	0·010	0·006	0·015	0·008	0·011	0·012	0·007	0·008	0·011	0·005	0·010	0·012	0·015
Total	4·005	4·004	4·001	4·006	4·011	4·008	4·001	4·001	3·996	3·997	3·989	4·008	4·000	3·980
Mol%														
X_{Mg}	81·7	71·0	86·2	66·2	87·8	79·0	82·2	71·6	86·8	79·6	84·0	76·4	81·5	71·3

	Clinopyroxene				Clinopyroxene				Clinopyroxene						Orthopyroxene			
	High-Zr	D9-R10			High-Zr	D15-R4			High-Zr	D19-R12					High-Zr	D9-R10		
	26-c	26-r	26-2-c	26-2-r	16-1-c	16-1-r	20-2-c	20-2-r	1-2-c	1-2-r	12-1- c	12-1-r	25-1-c	25-1-r	14-3-c	14-3-r	24-1-c	24-1-r
wt %																		
SiO_2	53·59	51·92	52·44	51·17	52·78	53·59	53·31	53·15	53·36	53·51	53·64	53·79	53·83	51·73	54·07	54·17	53·77	54·05
TiO_2	0·18	0·39	0·17	0·35	0·21	0·23	0·19	0·20	0·18	0·14	0·26	0·19	0·14	0·44	0·17	0·20	0·18	0·15
Al_2O_3	2·25	3·71	3·34	4·19	1·99	1·52	1·86	1·83	1·78	1·68	1·79	1·60	1·68	3·73	0·58	0·72	0·49	0·73
Cr_2O_3	0·02	0·05	0·24	0·00	0·08	0·07	0·09	0·04	0·07	0·06	0·08	0·04	0·06	0·14	0·03	0·00	0·01	0·00
FeO	6·50	8·16	4·60	7·00	7·57	8·30	8·24	8·39	6·94	8·46	7·49	8·39	6·51	8·16	21·09	21·33	21·97	20·09
MnO	0·17	0·23	0·11	0·15	0·25	0·28	0·28	0·26	0·23	0·26	0·24	0·25	0·19	0·22	0·91	0·90	1·11	0·87
MgO	16·89	16·24	16·38	15·38	16·89	17·69	17·87	17·91	17·19	17·80	17·46	17·78	17·08	15·47	22·39	22·53	21·32	22·84
CaO	21·16	19·24	22·77	21·27	19·25	17·96	17·95	17·56	19·98	17·82	19·67	18·28	21·02	20·23	1·37	1·43	1·56	1·38
Na_2O	0·13	0·16	0·12	0·13	0·15	0·11	0·14	0·12	0·11	0·11	0·11	0·11	0·10	0·20	0·03	0·04	0·05	0·02
Total	100·89	100·10	100·17	99·63	99·19	99·75	99·96	99·45	99·85	99·86	100·75	100·42	100·62	100·36	100·65	101·34	100·47	100·14
Cations (O = 6)																		
Si	1·948	1·911	1·916	1·894	1·955	1·970	1·957	1·960	1·960	1·966	1·955	1·966	1·962	1·906	1·993	1·986	1·998	1·993
Ti	0·005	0·011	0·005	0·010	0·006	0·006	0·005	0·006	0·005	0·004	0·007	0·005	0·004	0·012	0·005	0·006	0·005	0·004
Al	0·097	0·161	0·144	0·183	0·087	0·066	0·081	0·079	0·077	0·073	0·077	0·069	0·072	0·162	0·025	0·031	0·021	0·032
Cr	0·000	0·001	0·007	0·000	0·002	0·002	0·003	0·001	0·002	0·002	0·002	0·001	0·002	0·004	0·001	0·000	0·000	0·000
Fe	0·198	0·251	0·140	0·217	0·234	0·255	0·253	0·259	0·213	0·260	0·228	0·256	0·199	0·252	0·650	0·654	0·683	0·620
Mn	0·005	0·007	0·003	0·005	0·008	0·009	0·009	0·008	0·007	0·008	0·008	0·008	0·006	0·007	0·028	0·028	0·035	0·027
Mg	0·915	0·891	0·892	0·848	0·933	0·969	0·978	0·984	0·941	0·975	0·949	0·969	0·928	0·850	1·230	1·231	1·181	1·255
Ca	0·824	0·759	0·891	0·843	0·764	0·707	0·706	0·694	0·786	0·701	0·768	0·716	0·821	0·798	0·054	0·056	0·062	0·054
Na	0·009	0·012	0·008	0·009	0·011	0·008	0·010	0·008	0·008	0·008	0·007	0·008	0·007	0·014	0·002	0·003	0·003	0·002
Total	4·003	4·004	4·009	4·010	4·000	3·993	4·001	3·999	4·000	3·997	4·002	3·998	4·001	4·006	3·990	3·995	3·989	3·988
mol%																		
X_{Mg}	82·2	78·0	86·4	79·7	79·9	79·2	79·4	79·2	81·5	78·9	80·6	79·1	82·4	77·2	65·4	65·3	63·4	67·0

(continued)

Table 2: Continued

	Plagioclase						Plagioclase				Plagioclase			
	Low-Zr	29					Low-Zr	32			Low-Zr	35		
	5-c	5-r	7-p11-c	7-p11-r	1-p12-c	1-p12-r	p11-c	p11-r	p12-c	p12-r	30-p1-c	30-p1-r	32-p1-c	32-p1-r
wt %														
SiO_2	45·84	51·43	45·27	48·97	47·74	52·27	45·44	49·88	46·29	49·90	44·34	47·84	44·78	46·96
TiO_2	0·02	0·02	0·02	0·07	0·01	0·00	0·02	0·04	0·02	0·03	0·02	0·05	0·01	0·07
Al_2O_3	33·78	29·66	34·39	31·48	32·86	29·07	34·14	30·16	33·08	30·71	33·90	31·38	34·23	31·74
FeO*	0·76	1·24	0·56	0·84	0·84	1·21	0·59	1·04	0·65	0·95	0·61	0·82	0·58	0·87
MnO	0·00	0·02	0·00	0·01	0·01	0·02	0·02	0·00	0·02	0·00	0·02	0·02	0·03	0·00
MgO	0·14	0·16	0·09	0·21	0·16	0·20	0·08	0·29	0·14	0·24	0·07	0·19	0·07	0·17
CaO	18·78	14·91	19·17	16·22	17·36	14·04	18·97	15·57	18·08	15·71	19·00	16·75	19·06	17·11
Na_2O	0·86	2·91	0·56	2·26	1·55	3·33	0·76	2·38	1·11	2·45	0·50	1·37	0·45	1·32
K_2O	0·02	0·11	0·02	0·07	0·03	0·09	0·02	0·05	0·07	0·04	0·04	0·04	0·01	0·03
Total	100·21	100·52	100·07	100·13	100·59	100·24	100·03	99·39	99·45	100·03	98·49	98·47	99·22	98·27
Cations (O = 8)														
Si	2·117	2·344	2·093	2·247	2·186	2·381	2·102	2·301	2·149	2·287	2·085	2·231	2·088	2·200
Ti	0·001	0·001	0·001	0·002	0·000	0·000	0·001	0·001	0·001	0·001	0·001	0·002	0·000	0·003
Al	1·838	1·593	1·874	1·703	1·774	1·561	1·861	1·640	1·810	1·659	1·879	1·725	1·881	1·753
Fe	0·029	0·047	0·022	0·032	0·032	0·046	0·023	0·040	0·025	0·036	0·024	0·032	0·023	0·034
Mn	0·000	0·001	0·000	0·000	0·001	0·001	0·001	0·000	0·001	0·000	0·001	0·001	0·001	0·000
Mg	0·009	0·011	0·006	0·015	0·011	0·014	0·005	0·020	0·009	0·016	0·005	0·013	0·005	0·012
Ca	0·929	0·728	0·950	0·798	0·852	0·685	0·940	0·769	0·899	0·772	0·957	0·837	0·952	0·859
Na	0·077	0·257	0·050	0·201	0·138	0·294	0·068	0·212	0·100	0·218	0·045	0·124	0·041	0·120
K	0·001	0·006	0·001	0·004	0·002	0·005	0·001	0·003	0·004	0·002	0·002	0·003	0·001	0·002
Total	5·002	4·990	4·995	5·002	4·996	4·988	5·002	4·986	4·997	4·992	4·999	4·968	4·992	4·982
Mol%														
An	92·3	73·9	95·0	79·9	86·1	70·0	93·2	78·4	90·0	78·0	95·5	87·1	95·9	87·7

	Plagioclase				Plagioclase				Plagioclase					
	High-Zr	D9-R10			High-Zr	D15-R4			High-Zr	D19-R12				
	2 p1-c	2 p1-r	4 p1-c	4 p1-r	1-3 p1-c	1-3 p1-r	4-1 p1-c	4-1 p1-r	2-2 p1-c	2-2 p1-r	4-3 p1-c	4-3 p1-r	10-2 p1-c	10-2 p1-r
wt %														
SiO_2	45·03	44·91	45·68	52·24	45·11	50·64	46·81	49·78	46·24	47·75	45·71	47·38	45·52	47·24
TiO_2	0·00	0·01	0·02	0·14	0·00	0·02	0·00	0·04	0·01	0·03	0·00	0·01	0·02	0·01
Al_2O_3	34·18	34·63	34·34	27·10	34·14	29·32	32·73	30·69	33·42	32·85	33·98	32·48	34·37	32·50
FeO*	0·60	0·72	0·48	3·10	0·60	1·12	0·72	0·86	0·64	0·78	0·59	0·81	0·52	0·80
MnO	0·00	0·02	0·01	0·04	0·01	0·01	0·05	0·01	0·00	0·03	0·01	0·00	0·00	0·00
MgO	0·08	0·08	0·03	1·31	0·08	0·13	0·13	0·21	0·12	0·18	0·09	0·17	0·09	0·17
CaO	18·23	18·54	18·86	13·33	18·60	14·57	17·40	15·27	17·69	17·21	18·54	17·18	19·00	17·27
Na_2O	0·66	0·68	0·90	2·49	0·74	3·09	1·43	2·71	1·18	1·64	0·79	1·58	0·75	1·60
K_2O	0·05	0·06	0·04	0·12	0·02	0·14	0·02	0·05	0·02	0·03	0·02	0·04	0·01	0·03
Total	98·85	99·66	100·39	99·93	99·33	99·08	99·29	99·65	99·33	100·52	99·77	99·65	100·30	99·63
Cations (O = 8)														
Si	2·103	2·084	2·104	2·402	2·099	2·342	2·173	2·289	2·145	2·187	2·116	2·190	2·099	2·185
Ti	0·000	0·000	0·001	0·005	0·000	0·001	0·000	0·001	0·000	0·001	0·000	0·000	0·001	0·000
Al	1·881	1·894	1·864	1·468	1·873	1·598	1·790	1·663	1·828	1·773	1·854	1·769	1·867	1·772
Fe	0·023	0·028	0·018	0·119	0·023	0·043	0·028	0·033	0·025	0·030	0·023	0·031	0·020	0·031
Mn	0·000	0·001	0·001	0·002	0·000	0·000	0·002	0·001	0·000	0·001	0·000	0·000	0·000	0·000
Mg	0·005	0·005	0·002	0·090	0·005	0·009	0·009	0·014	0·008	0·012	0·006	0·012	0·006	0·012
Ca	0·912	0·922	0·931	0·656	0·927	0·722	0·865	0·753	0·880	0·845	0·919	0·851	0·939	0·856
Na	0·060	0·061	0·081	0·222	0·066	0·277	0·129	0·242	0·106	0·145	0·071	0·141	0·067	0·144
K	0·003	0·004	0·002	0·007	0·001	0·008	0·001	0·003	0·001	0·001	0·001	0·002	0·001	0·002
Total	4·988	5·000	5·005	4·973	4·997	5·001	4·997	5·000	4·994	4·998	4·992	4·997	5·000	5·002
mol%														
An	93·8	93·8	92·0	74·7	93·3	72·3	87·1	75·7	89·2	85·3	92·9	85·8	93·4	85·6

c, core; r, rim.

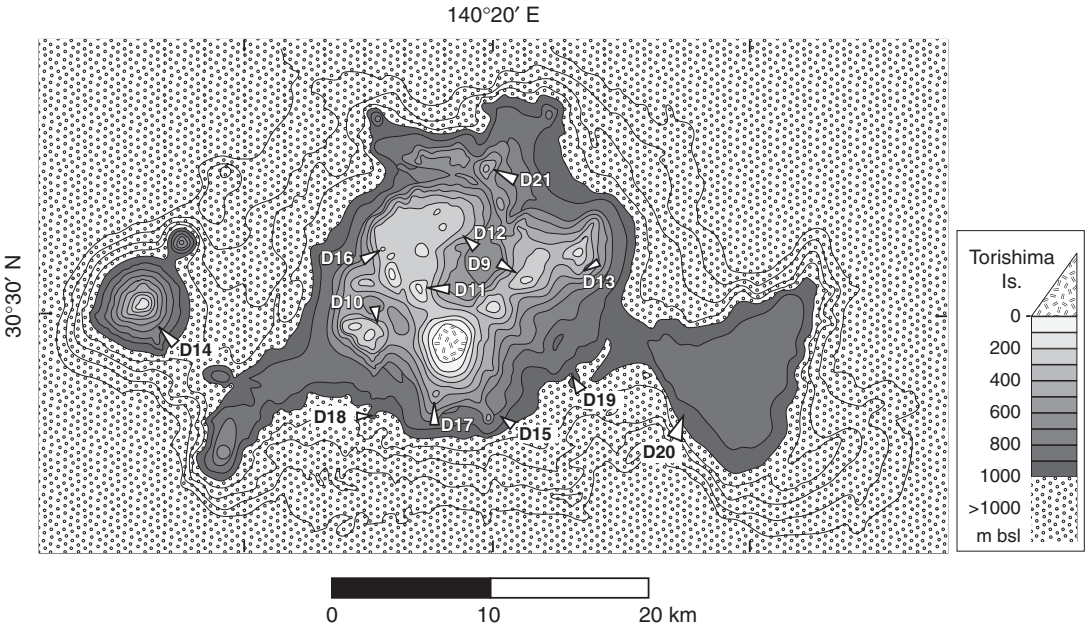

Fig. 2. Bathymetric map of the Torishima volcano. Numbered arrows (D9–D21) are sites dredged by the R.V. *Kairei* in December 2002. The main body of Torishima volcano, 20 km in diameter, rises from an ocean depth of about 1000 m. Torishima island, which lies astride the south rim of Torishima submarine caldera, was studied and sampled in 2003.

by XRF. Torishima seamount (D14 in Fig. 2), an isolated knoll 20 km west of Torishima island, consists of andesite and dacite scoriae (60·7–66·6 wt % SiO_2) characterized by systematically higher TiO_2 and K_2O contents than Torishima volcano at a given SiO_2 content. Thus, the Torishima knoll is not considered to be part of the Torishima magmatic system and is not considered further. Most of Torishima island consists of older prehistoric lavas and dykes (<50 wt % SiO_2), which are overlain by younger prehistoric lavas (~51–53 wt % SiO_2) and then by basaltic andesite lava flows of the 1939 eruption (~54·5 wt % SiO_2) (Table 1, Fig. 3).

Collectively, more than 70% of the samples from Torishima volcano are basalts and basaltic andesite lava flows and dykes (<55% SiO_2). Samples containing >55 wt % SiO_2 consist mostly of scoria and pumice and were collected both on land and in dredge hauls from the nearby sea floor. Figure 4 shows the variation of MgO vs SiO_2 for the analysed samples from Sumisu and Torishima volcanoes. Both volcanoes display compositions ranging from basalt to rhyolite. At Sumisu, a ~6 wt % SiO_2 gap separates andesites from dacites [see Shukuno *et al.* (2006) for a possible explanation of this gap]; at Torishima, pumices from the both the sea floor and the island bridge this gap (Fig. 4).

Basalts from Torishima volcano

Torishima contains two types of basalt, comparison between which provides important insights into the role of slab-derived components in arc-front basalt genesis.

The volcano is made up of three basalt groups of differing ages, which are separated by two small, but well-defined, gaps in SiO_2 (50–51 wt % and 53–54·5 wt %) (Fig. 5a). Silica content increases from the older prehistoric units (<50 wt % SiO_2) through the younger prehistoric units (~51–53 wt % SiO_2) to the products of the 1939 eruption (54·5 wt % SiO_2) (Figs 3 and 5a). Our field study of Torishima island suggests that the main body of the island, and possibly the entire Torishima volcano, consists of older prehistoric lavas and dykes (Fig. 3). Thus, basalts containing <50 wt % SiO_2 are the most voluminous. Using FeO^*/MgO as a proxy for differentiation, however, the basalts form two trends, which are distinguished by their differing Zr contents at the same FeO^*/MgO (Fig. 5b). Basalts with $SiO_2 < 50$ wt % have lower Zr at the same FeO^*/MgO than basalts and basaltic andesites with >51 wt % SiO_2, which are comparable respectively to the low-Zr and high-Zr basalts of Sumisu (Tamura *et al.*, 2005). Most basaltic volcanism in Torishima volcano, therefore, consists of low-Zr basalts, which change to high-Zr basalts in the later stages of activity without apparent mixing (Fig. 5b).

Our data for the Torishima island basalts are comparable with those of Taylor & Nesbitt (1998) and Gill *et al.* (1994). The data of Taylor & Nesbitt (1998) encompass the range of our low-Zr basalts to high-Zr basalts whereas Gill *et al.* (1994) reported data for the high-Zr basalt that erupted in 1939.

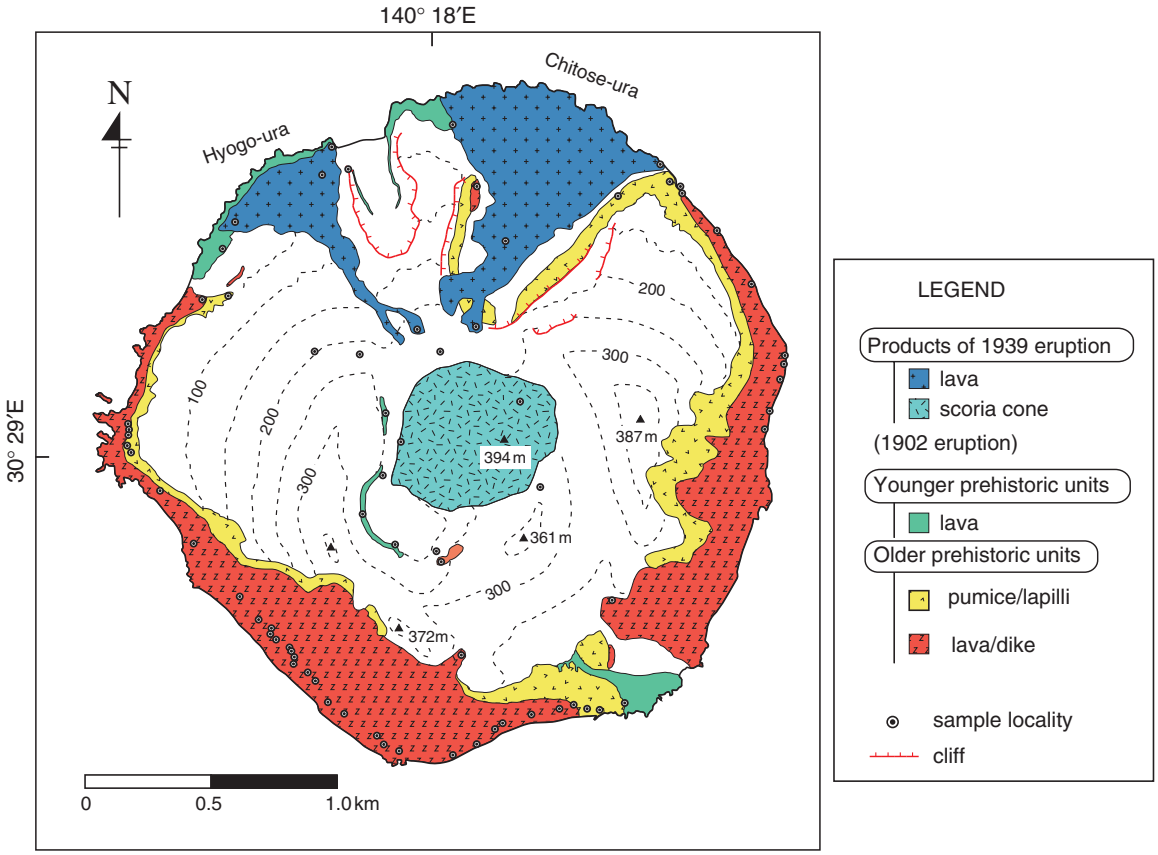

Fig. 3. Geological map of Torishima island, simplified from N. Isshiki (unpublished data). Dots show sites sampled in 2003. The white fill pattern indicates areas where no outcrops are observed.

PETROGRAPHY AND OLIVINE CHEMISTRY OF LOW-ZR AND HIGH-ZR BASALTS FROM TORISHIMA VOLCANO

Figure 6 shows mineral assemblages and modes (vol.%) of 37 high-Zr basalts and 93 low-Zr basalts, in order of increasing FeO^*/MgO. The FeO^*/MgO values of the low-Zr basalts and high-Zr basalts from Torishima have similar ranges from 1·31 to 2·78 and from 1·13 to 2·68, respectively. Most low-Zr basalts, however, have FeO^*/MgO <2, whereas many of the high-Zr basalts are more differentiated and have FeO^*/MgO >2.

With respect to mafic mineral phenocrysts, 90 of 93 low-Zr basalts contain both olivine and augite. Two samples, with 1·8–1·9 FeO^*/MgO, contain only olivine phenocrysts; the most differentiated sample ($FeO^*/MgO = 2·78$) contains orthopyroxene and augite phenocrysts without olivine. In contrast, the high-Zr basalts show a wider variation in mafic phenocryst assemblages. Fifteen of 37 high-Zr basalts contain olivine + augite, nine contain olivine + augite + orthopyroxene, nine contain augite + orthopyroxene, two contain only augite, and one sample each contains only olivine or orthopyroxene. Four samples, with FeO^*/MgO <2·0, contain orthopyroxene phenocrysts, suggesting earlier crystallization of orthopyroxene in high-Zr basalts. No pigeonite has been observed as a phenocryst in either the low-Zr basalts or high-Zr basalts.

Figure 7 shows olivine, plagioclase, orthopyroxene, clinopyroxene, and 'total phenocrysts' contents (vol.%) vs FeO^*/MgO in the whole-rocks. The phenocryst content of the low-Zr basalts ranges from 27 to 51%, averaging ~40%. The phenocryst content of high-Zr basalts averages ~30 vol.%, about 10% lower than for the low-Zr basalts. Moreover, many high-Zr rocks contain <20 vol.% of phenocrysts, and one sample ($FeO^*/MgO = 2·0$) is aphyric (~1% phenocrysts). Generally, the low-Zr basalts contain more abundant phenocrysts than the high-Zr basalts, but orthopyroxene appears only in the high-Zr basalts at FeO^*/MgO <2. Plagioclase abundances are similar in the low-Zr and high-Zr basalts, except in some phenocryst-poor rocks and in the 1939 lava flows (Fig. 7).

At Sumisu, many high-Zr basalts contain only olivine + plagioclase, and augite appears only in the more

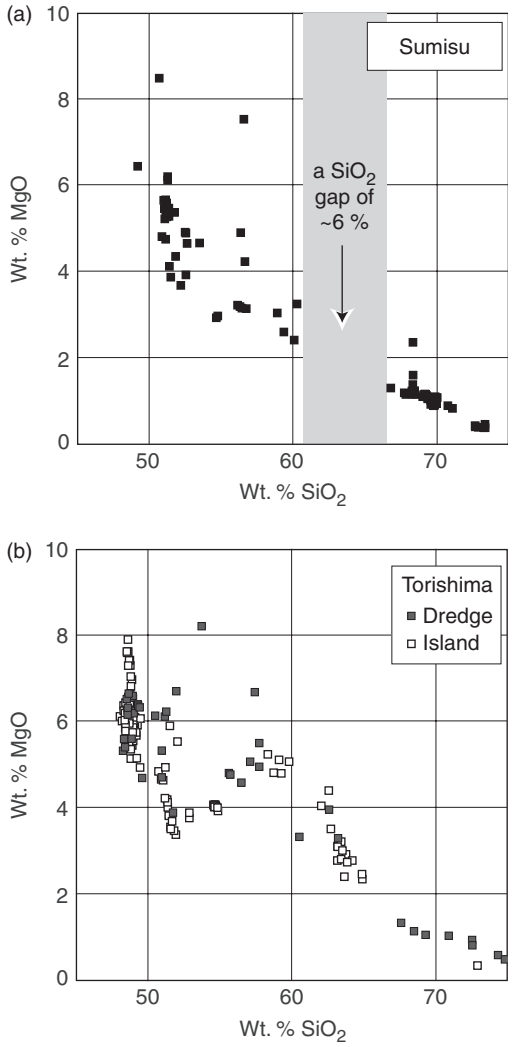

Fig. 4. MgO vs SiO_2 variation in lava flows from (a) Sumisu and (b) Torishima.

evolved lavas of the high-Zr basalts. Most Torishima high-Zr basalts, however, contain augite phenocrysts. Figure 8 shows photomicrographs of Torishima basalts and basaltic andesites. Some plagioclases in low-Zr basalts contain inclusions of augite (Fig. 8a), whereas, in contrast, some augites in the high-Zr basalts contain inclusions of plagioclase (Fig. 8b and c). Augite phenocrysts containing plagioclase inclusions have not been observed in the low-Zr basalts. The presence or absence of plagioclase inclusions in augite or vice versa may not necessarily provide strong evidence of the order of crystallization, and the inclusions could be xenocrystal. We consider it likely that augite crystallized after plagioclase in the Torishima high-Zr basalts. It is possible that the crystallization sequences of the high-Zr basalts in both Sumisu and Torishima are the same, but they differ from those of the low-Zr basalts in these two areas.

Olivines

Olivine phenocrysts occur in both the low- and high-Zr basalts from Torishima (Figs 6 and 7). Figure 9 shows the variation of NiO vs Fo [100Mg/(Mg + Fe)]. The low-Zr basalts are richer in olivine phenocrysts than the high-Zr basalts (Fig. 7), but both low- and high-Zr basalts have similar olivine compositions in terms of Fo and NiO contents (Fig. 9a). Low-Zr Torishima basalts contain as much as 7 vol.% olivine (Fig. 7), but the NiO contents of these olivines are low (Fig. 9a), suggesting a high degree of olivine fractionation before eruption. At Sumisu, olivines in the low-Zr basalts have lower NiO contents and/or have higher Fo values than those in the high-Zr basalts at given Fo and NiO contents, respectively. Based on this olivine chemistry, Tamura *et al.* (2005) suggested that low-Zr basalts are the products of higher degrees of partial melting than the high-Zr basalts. Unfortunately, all olivines from Torishima are fairly evolved, and most basalts contain augite phenocrysts. Thus the differences in olivine chemistry between the primary low-Zr and high-Zr basalts have been obscured by fractionation of both olivine and augite.

We selected the most magnesian low-Zr basalts (31, 33, 35.5, 103 and 117) and high-Zr basalts (11, D15-R7, D19-R10, D19-R12 and D19-R13) to minimize the effect of augite fractionation. Figure 9b shows the composition of olivine phenocrysts in the low-Zr basalts (red field) and high-Zr basalts (blue field) compared with calculated equilibrium olivines (squares) and olivine fractionation trends (lines) determined for magnesian low-Zr basalts (black squares; 31, 33, 35.5, 103 and 117) and magnesian high-Zr basalts (white squares; 11, D15-R7, D19-R10, D19-R12 and D19-R13). The numbers on the lines indicate the percentage of added equilibrium olivine. Calculated olivine compositions in the low-Zr basalts are more magnesian than those in high-Zr basalts at a given NiO content. Low-Zr basalts contain olivine phenocrysts whose compositions overlap those of the calculated equilibrium olivines, and continuously extend towards more iron-rich compositions with decreasing NiO content and also extend to more iron-rich compositions at the same NiO content. The latter could be the effect of the augite fractionation. On the other hand, although the high-Zr basalts contain several olivine phenocrysts that are more magnesian than the calculated equilibrium olivines, most olivine compositions from the high-Zr basalts overlap those of the calculated equilibrium olivines and continuously extend toward more iron-rich compositions. It is possible that several magnesian olivines, which are more magnesian than the equilibrium high-Zr olivine trends, could be xenocrysts from older low-Zr basalt magmas because the majority of actual

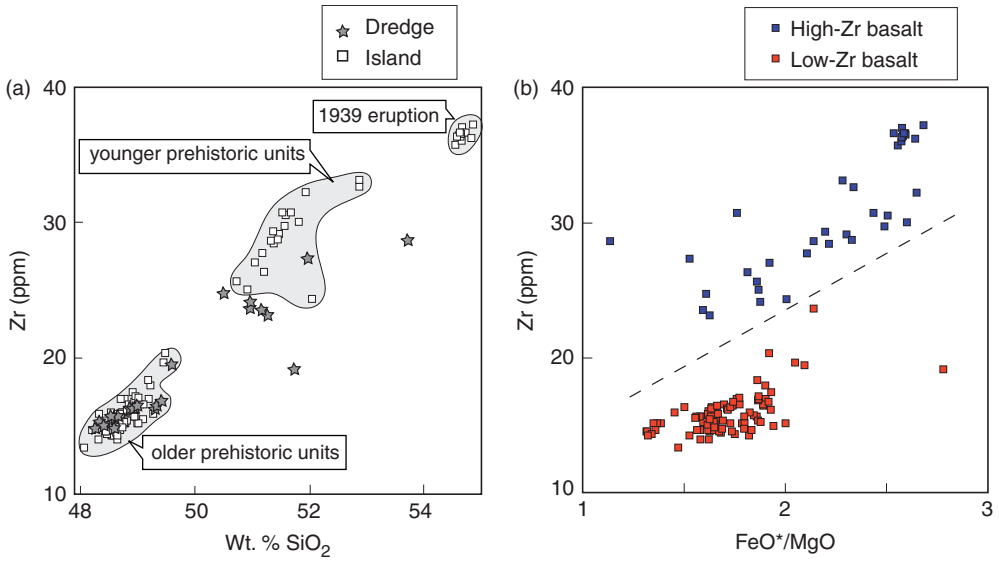

Fig. 5. (a) Zr vs SiO_2 variation for Torishima basalts. Torishima is composed of three groups of basaltic lavas, separated by small, but clear, gaps in SiO_2 content (<50 wt %, ~51–53 wt %, and ~54·5 wt % SiO_2). (b) Zr vs FeO*/MgO. Using FeO*/MgO as a proxy for differentiation, the Torishima basalts form two trends distinguished by their different Zr contents at the same FeO^*/MgO, which are comparable with the low-Zr and high-Zr basalts of Sumisu (Tamura *et al.*, 2005).

high-Zr basalt olivines plot on the extension of the calculated high-Zr basalt olivine trends. The primary olivine compositions at 0·4 wt % NiO calculated for the low-Zr basalts (31, 33, 35.5, 103 and 117) range from $Fo_{92·8}$ to $Fo_{93·3}$, with an average of Fo_{93}. In contrast, those calculated for the high-Zr basalts (11, D15-R7, D19-R10, D19-R12 and D19-R13) are Fo_{91} on average and range from $Fo_{90·3}$ to $Fo_{91·4}$. Thus, we can conclude from Fig. 9 and the primary olivine compositions calculated from the whole-rock compositions [see Tamura *et al.* (2005) for details], that both low-Zr and high-Zr basalts were derived from depleted, and thus magnesiun-rich, mantle sources and that the source mantle of the low-Zr basalts is more magnesian, and thus more depleted, than that of the high-Zr basalts.

GEOCHEMISTRY OF LOW-Zr VS HIGH-Zr BASALTS FROM TORISHIMA VOLCANO

Figure 10 shows the variation of selected major elements (SiO_2, Al_2O_3, MgO, TiO_2, FeO^*, CaO, Na_2O and K_2O; Fig. 10a) and trace elements (Ni, Sr, Y, Rb, Cu and Zn; Fig. 10b) vs FeO^*/MgO in the high-Zr and low-Zr Torishima basalts. The K_2O contents of the high-Zr basalts are almost twice those of the low-Zr basalts at the same FeO^*/MgO. SiO_2, Na_2O, Cu and Y also show systematic differences between these two basalt types, but on smaller scales. They do not display systematic differences in Al_2O_3, MgO, TiO_2, Ni, Sr, and Zn at a given FeO^*/MgO.

All Torishima basalts are strongly depleted in light REE (LREE), compared with middle REE (MREE) and heavy REE (HREE) (Fig. 11). Importantly, the low-Zr basalts at Torishima are more LREE depleted than the high-Zr basalts, a feature also observed at Sumisu volcano (Tamura *et al.*, 2005). Figure 11 shows that the REE patterns of the low-Zr and high-Zr basalts from Torishima are comparable with those at Sumisu.

Figure 12 shows the variation of La/Sm vs Gd/Yb and La/Sm vs Zr/Y for Torishima (this study) and Sumisu (Tamura *et al.*, 2005). La/Sm is positively correlated with Gd/Yb and Zr/Y at both Torishima and Sumisu, and the ranges and values are similar. La/Sm values at Sumisu range from 0·7 to 1·05, and the low-Zr basalts have lower ratios, ranging from 0·7 to 0·9. At Torishima, La/Sm values range from 0·7 to 1·0, and, again, the low-Zr basalts in Torishima have lower ratios, ranging from 0·7 to 0·8. It is important to note, however, that although the shapes of the REE patterns are similar (Fig. 11), the absolute REE concentrations are lower in the Torishima low-Zr suite than in the Sumisu low-Zr suite. The low-Zr suite of basalts are amongst the most LREE-depleted basalts found anywhere on Earth to date, despite having experienced differentiation that has given rise to whole-rock MgO contents ranging from 7·6 to 5·0 wt % and olivines with Fo_{85} to Fo_{65}. The extreme depletion is indicated by the rocks having less than five times the mantle concentrations of HREE and HFSE and sub-chondritic Nb.

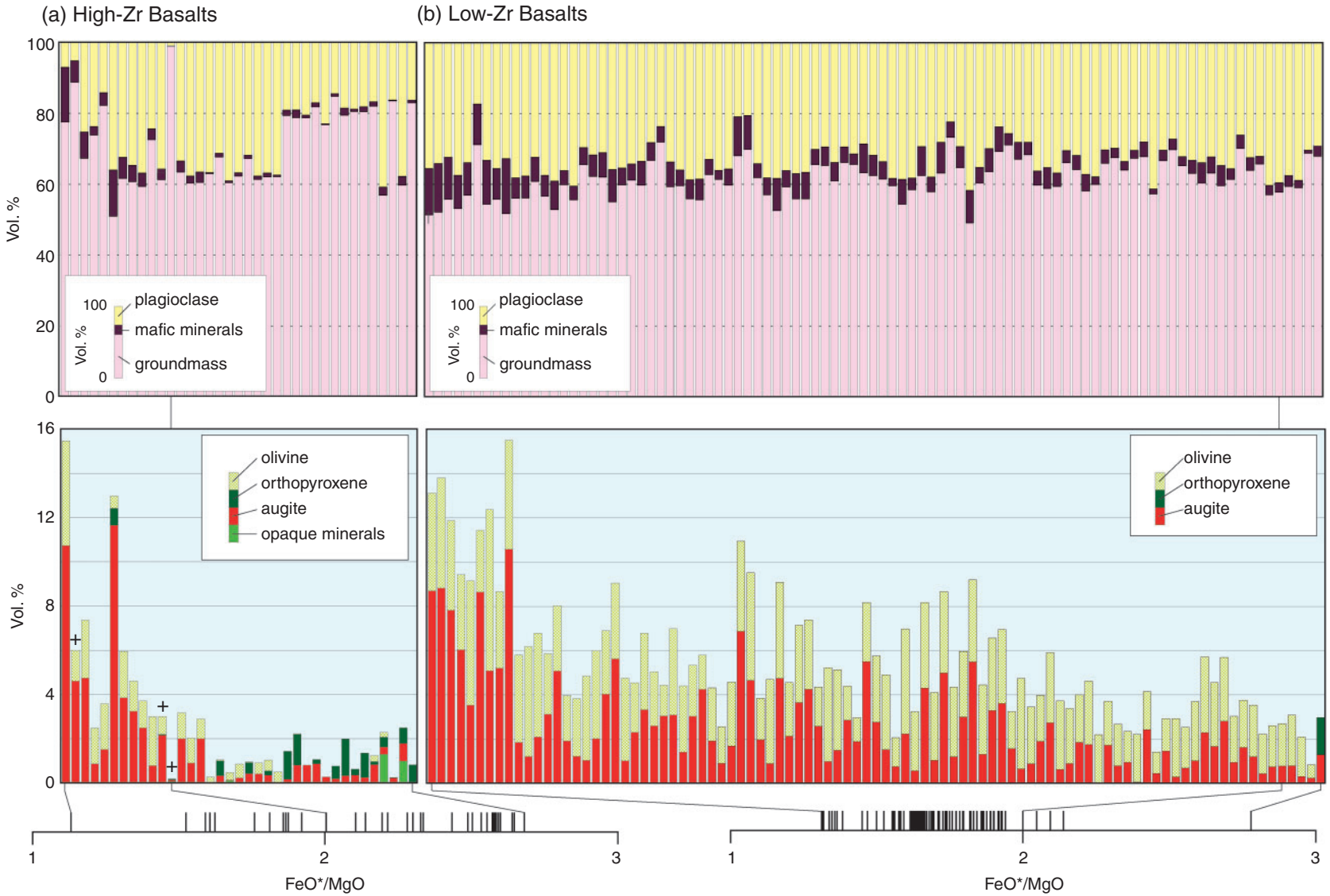

Fig. 6. Mineral assemblages and modes (vol.%) of 37 high-Zr basalts and 93 low-Zr basalts in order of increasing FeO^*/MgO. The actual FeO^*/MgO is shown at the bottom of the histograms. Mode (vol.%) of phenocrysts based on 4000–5000 points counts. FeO^*/MgO ranges from 1·13 to 2·68 in the high-Zr basalts and from 1·31 to 2·78 in the low-Zr basalts. The upper and lower diagrams in each basalt group respectively show the modes of plagioclase, mafic minerals and groundmass and modes of olivine, orthopyroxene, augite and opaque minerals. The rare orthopyroxene phenocrysts in the high-Zr basalts are shown by crosses (+).

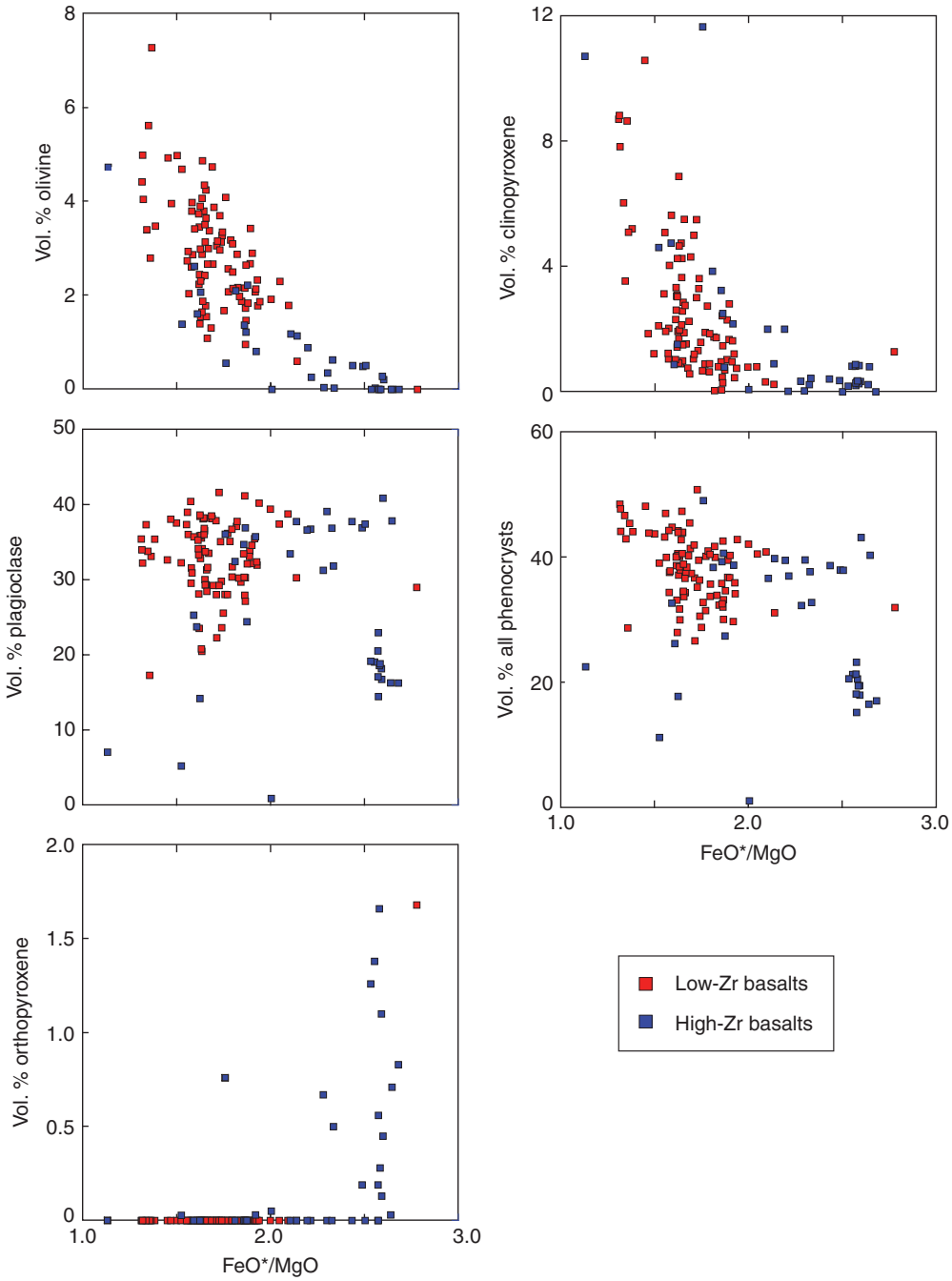

Fig. 7. FeO∗/MgO variation diagrams comparing low-Zr basalts with high-Zr basalts in terms of phenocryst contents of olivine, clinopyroxene, plagioclase, 'all phenocrysts' and orthopyroxene.

Furthermore, their incompatible element concentrations are about half of the concentrations in the most depleted mid-ocean ridge basalt (MORB) known, despite being more differentiated. Such extremely depleted rocks have been found in only one other area, the northernmost islands of Tonga, especially on Tafahi (J. B. Gill, personal communication).

DEGREES OF MELTING OF THE SOURCE OF THE TORISHIMA BASALTS

The degree of partial melting of the source of the primary magmas can be estimated using the ratios of trace element concentrations in lavas with different compositions, as has

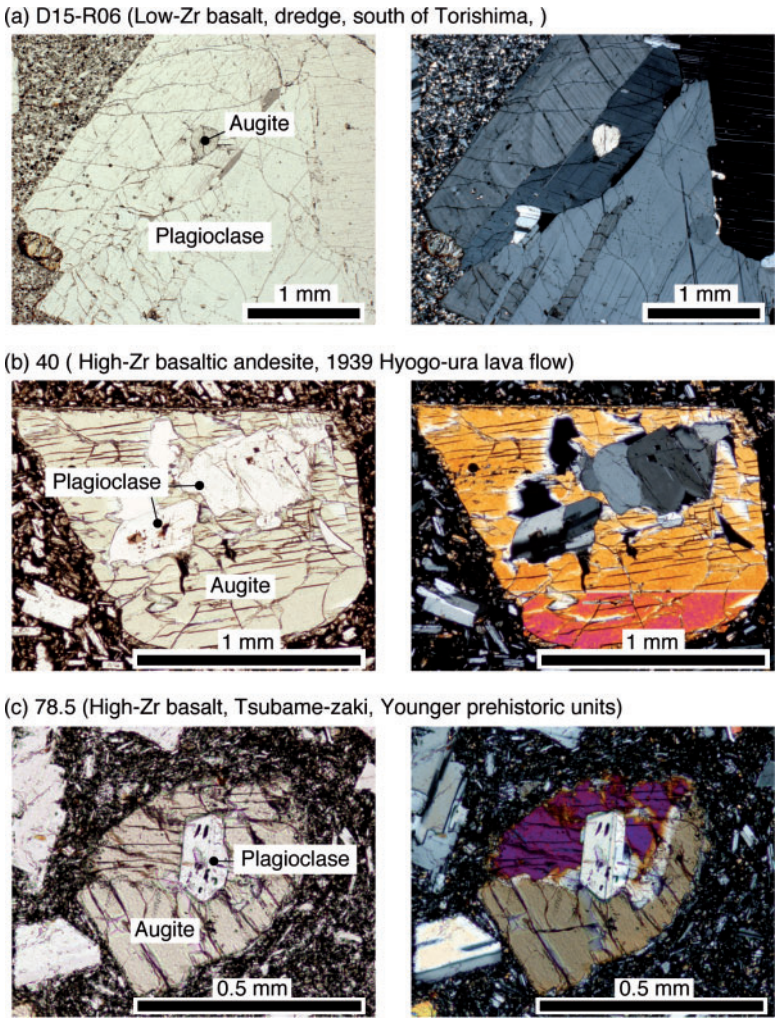

Fig. 8. Photomicrographs of Torishima basalts and basaltic andesite, under plane-polarized light and crossed polars. (a) Plagioclase phenocryst in low-Zr basalt D15-R06 contains an augite phenocryst, suggesting earlier crystallization of augite in the low-Zr basalt magma. (b, c) Augite phenocrysts in high-Zr basaltic andesite 40 and basalt 78.5 contain plagioclase phenocrysts. In contrast to low-Zr basalts, augite crystallizes after plagioclase in the high-Zr basalt magma.

been described by Maaløe (1994) and Maaløe & Pedersen (2003). To accomplish this, those workers assumed (1) the likely modal mineralogy of the source mantle, and (2) the relative proportions of the mineral constituents that enter the melt. Based on these assumptions, the estimated degree of melting depends on the trace element ratios in two selected lava compositions and not on their absolute values. Tamura *et al.* (2005) constrained the degree of melting of the source mantle beneath Sumisu using three ratios (La/Sm, Sm/Yb, and Zr/Y) in lavas of differing composition without making the two assumptions listed above. Although they were unable to obtain unique solutions, some consistent constraints emerged.

Here, we better constrain the degree of partial melting of the source of the primary magmas, using La/Sm in lavas of differing composition and making the two assumptions listed above. This approach, assuming that the effects of slab-derived components on LREE abundances are minimal, is tenable at Sumisu and Torishima because (1) the lavas of both volcanoes are heavily depleted in LREE compared with MREE and HREE (Fig. 11), and (2) La/Sm is positively correlated with Gd/Yb and Zr/Y in both the Torishima and Sumisu basalts (Fig. 12). First, we assume that the relative proportions of the mineral constituents enter the melt according to the reaction of Gaetani & Grove (1998), for non-modal batch melting of hydrous lherzolite at 1·2 GPa: 0·62 cpx + 0·51 opx + 0·12 sp = 0·25 ol + 1·0 melt. Second, although the Izu–Bonin arc basalts are among the most depleted on Earth, we assume that residual clinopyroxene plays a major role in fractionating La from Sm and Zr from Y

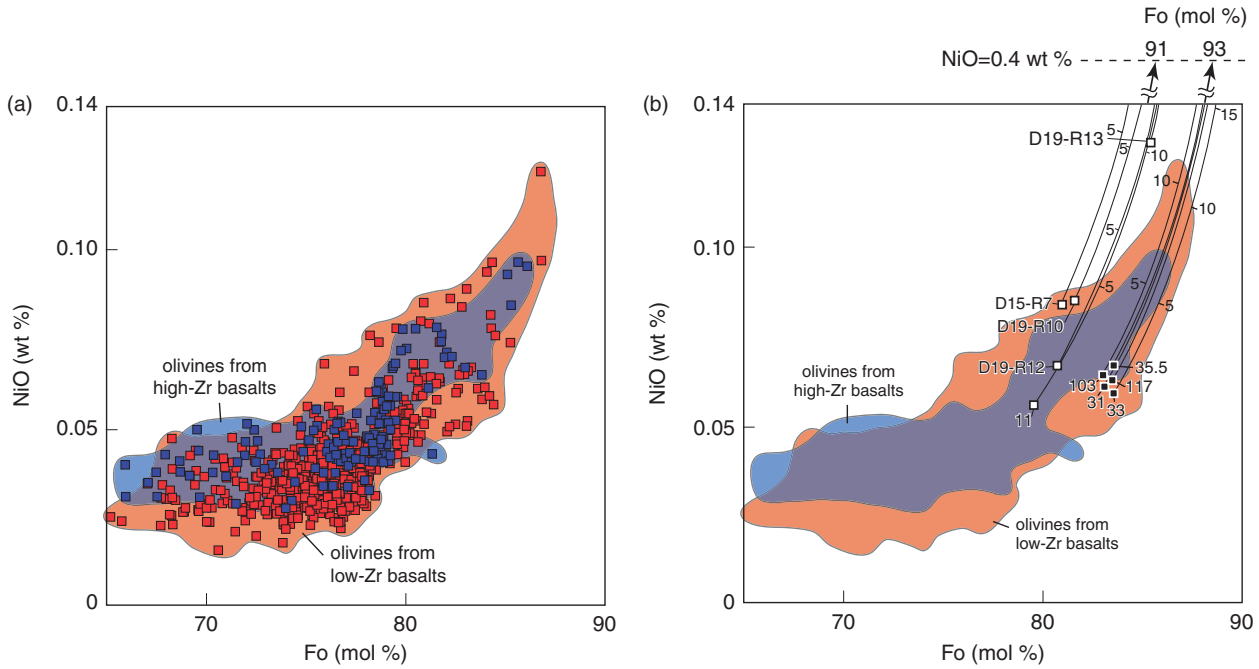

Fig. 9. Variation of NiO wt % vs Fo mol% [100Mg/(Mg + Fe)] for olivine phenocrysts in Torishima basalts. (a) Observed olivines from low-Zr basalts (samples 29, 32, 35, 64, 69, 89, 99 and 140) (red squares) and those from high-Zr basalts (D9-R10, D15-R04 and D19-R12) (blue squares). (b) Olivine phenocrysts in low-Zr basalts (red field) and high-Zr basalts (blue field) compared with calculated equilibrium olivines (squares) and olivine fractionation trends (lines) determined for magnesian low-Zr basalts (black squares; 31, 33, 35. 5, 103 and 117) and magnesian high-Zr basalts (white squares; 11, D15-R7, D19-R10, D19-R12 and D19-R13). The numbers on the lines indicate the percentage of added equilibrium olivine. Calculated olivines in the low-Zr basalts are more magnesian than those in high-Zr basalts at a given NiO content. The primary olivine compositions at 0·4 wt % NiO calculated for the low-Zr and high-Zr basalts are Fo_{93} and Fo_{91} on average, respectively. The olivine fractionation model of Tamura *et al.* (2000), which was revised by W. P. Leeman in 2004, is available from the author for use in Microsoft® Excel©.

(Tamura *et al.*, 2005). Thus the melting residues of the Izu–Bonin basalts could range from cpx-free harzburgite to lherzolite containing small amounts of clinopyroxene. Hirschmann *et al.* (1999) showed that when cpx is exhausted from the residue during isobaric batch melting of spinel peridotite at 1 GPa, the isobaric productivity calculated by MELTS decreases by more than a factor of four, and therefore extensive partial melting of harzburgitic residues is inhibited. Thus, we assume that all clinopyroxene could be exhausted to leave a harzburgitic residue in the source of the low-Zr primary basalts. This residue is just at the point of the cpx-out reaction without further melting of the harzburgitic residue, when the melt fraction is 0·2.

Gaetani *et al.* (2003) and McDade *et al.* (2003*a*) showed that under both hydrous and anhydrous conditions, there are differences in the partitioning behaviour of trace elements during mantle melting. For hydrous harzburgite, which is assumed to be the residue of the primary low-Zr basalts, hydrous melting partition coefficients for orthopyroxene are taken from McDade *et al.* (2003*a*); these are similar to the anhydrous ones of McDade *et al.* (2003*b*). Those for olivine are taken from McDade *et al.* (2003*b*), assuming that H_2O has a negligible effect on olivine–melt partition coefficients. Residual clinopyroxene plays a major role in fractionating La from Sm, and thus the residue of the primary high-Zr basalts should contain some clinopyroxene. Although the high-Zr basalts are not thought to be dry, they should contain less water than the low-Zr basalts. As a result, for the source mantle of the high-Zr basalts, anhydrous melting partition coefficients, taken from McDade *et al.* (2003*b*), are used for olivine, clinopyroxene and orthopyroxene. When the olivine content of the residue of the high-Zr basalts is assumed to be more than 70 wt %, the likely modal mineralogy of the original mantle can be determined. Spinel is not included in the calculations because spinel–melt partition coefficients are assumed to be negligible for La and Sm.

Interactive calculations were performed to minimize the difference between the original mantle source mineralogy (olivine, orthopyroxene and clinopyroxene) of the low-Zr basalts and that of the high-Zr basalts.

Following Tamura *et al.* (2005),

$$F^{\mathrm{H}} = -\frac{\gamma + 0\cdot 2\varepsilon}{\alpha + 0\cdot 2\beta}$$

when

$$\alpha = a(1 - D^{\mathrm{H}}_{\mathrm{Sm}})D^{\mathrm{L}}_{\mathrm{La}} - (1 - D^{\mathrm{H}}_{\mathrm{La}})D^{\mathrm{L}}_{\mathrm{Sm}}$$

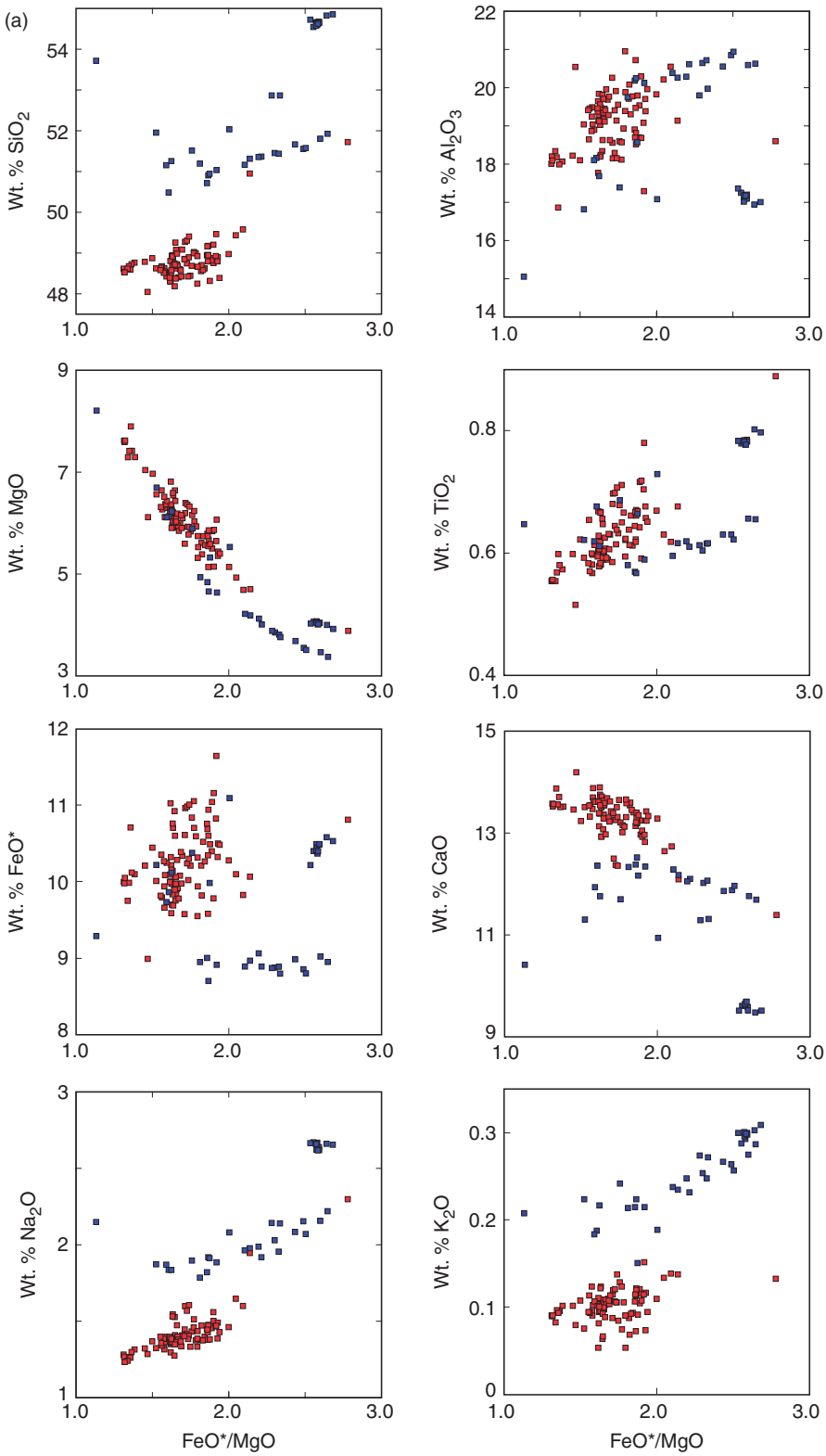

Fig. 10. Chemistry of Torishima high-Zr and low-Zr basalts. (a) Major elements (SiO_2, Al_2O_3, MgO, TiO_2, FeO*, CaO, Na_2O, K_2O) and (b) trace elements (Ni, Sr, Y, Rb, Cu and Zn) vs FeO*/MgO.

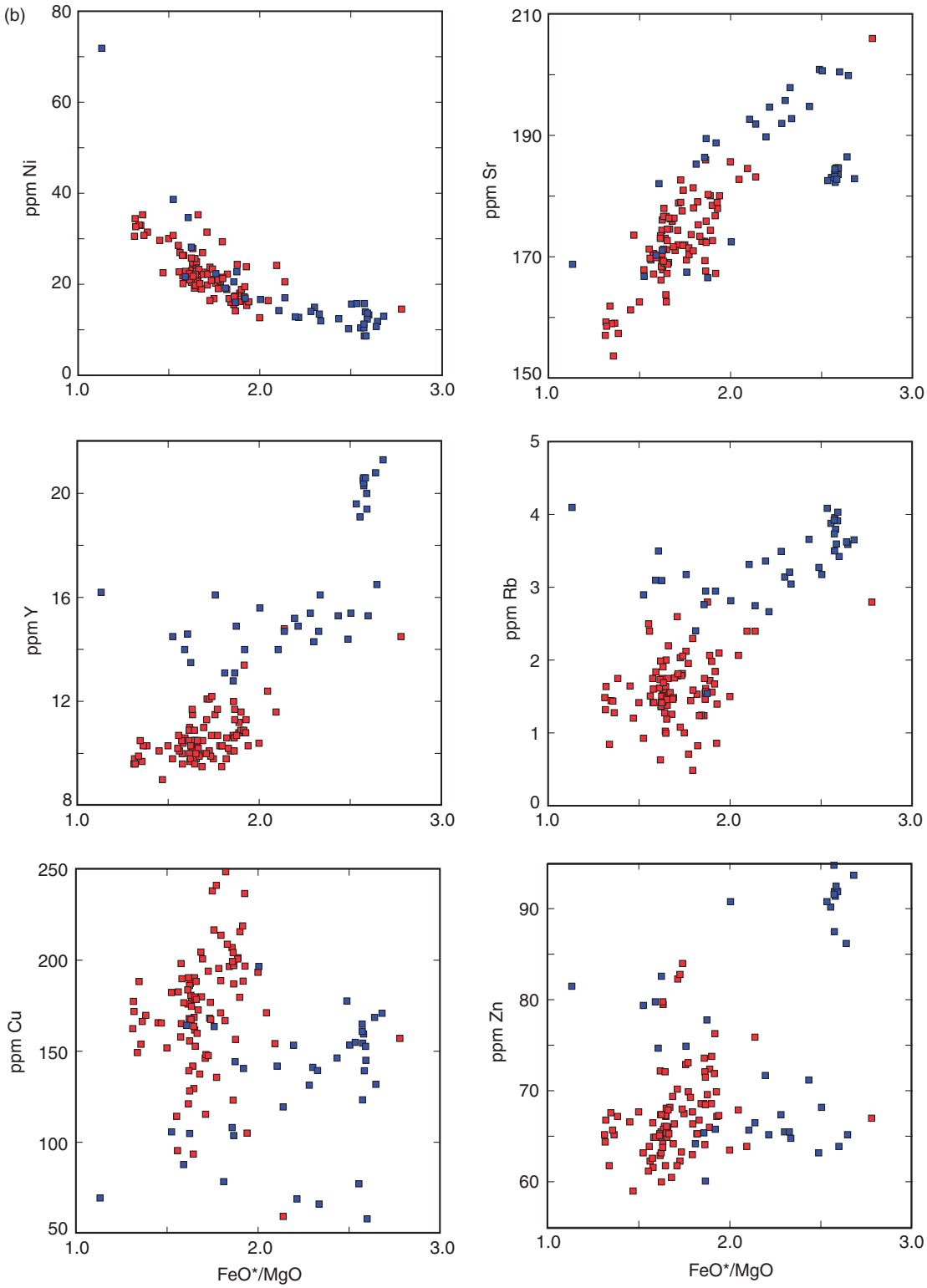

Fig. 10. Continued.

$$\beta = a(1 - D^{L}_{La})(1 - D^{H}_{Sm}) - (1 - D^{L}_{Sm})(1 - D^{H}_{La})$$

$$\gamma = aD^{L}_{La}D^{H}_{Sm} - D^{H}_{La}D^{L}_{Sm}$$

$$\varepsilon = a(1 - D^{L}_{La})D^{H}_{Sm} - (1 - D^{L}_{Sm})D^{H}_{La}$$

$$a = \frac{La^{L}}{Sm^{L}} \cdot \frac{Sm^{H}}{La^{H}}$$

where superscript L and H denote low-Zr basalt and high-Zr basalt, respectively, D is the bulk distribution coefficient between the respective primary magma and its residue, and F the degree of partial melting. The concentrations of La and Sm are in ppm. The proportions of olivine and orthopyroxene in the residue of the low-Zr basalt and those of olivine, orthopyroxene, clinopyroxene in the residue of the high-Zr basalt could be variable. Bulk partition coefficients depend on the modal mineralogy. F^{H} depends on the bulk partition coefficients and the La/Sm ratios of low-Zr and high-Zr basalts. The modal mineralogy of both residues, however, cannot change independently. The mode of the original mantle is obtained by adding residues and the

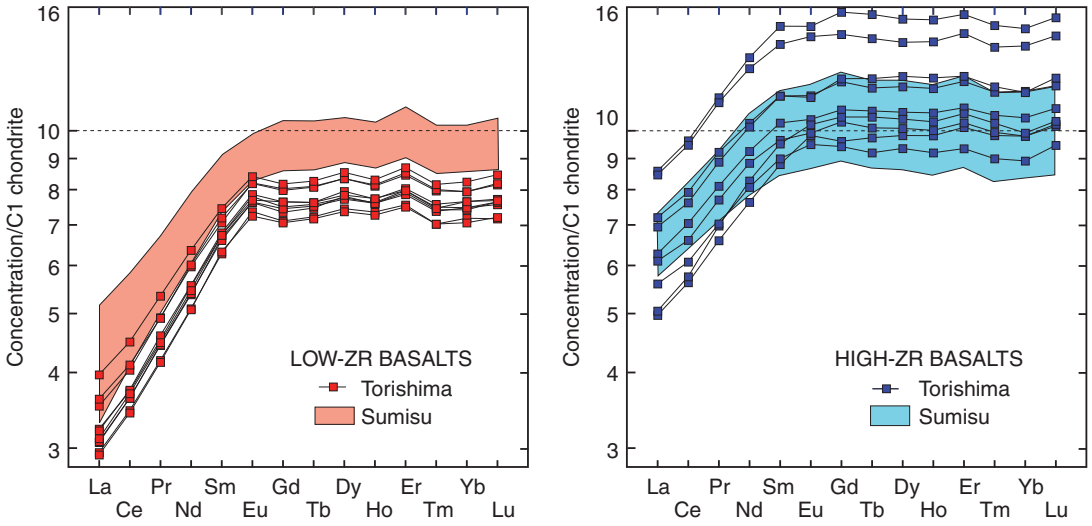

Fig. 11. Rare earth element (REE) patterns of Torishima low-Zr and high-Zr basalts compared with Sumisu low- and high-Zr basalts. Cl chondrite composition is that of Sun & McDonough (1989).

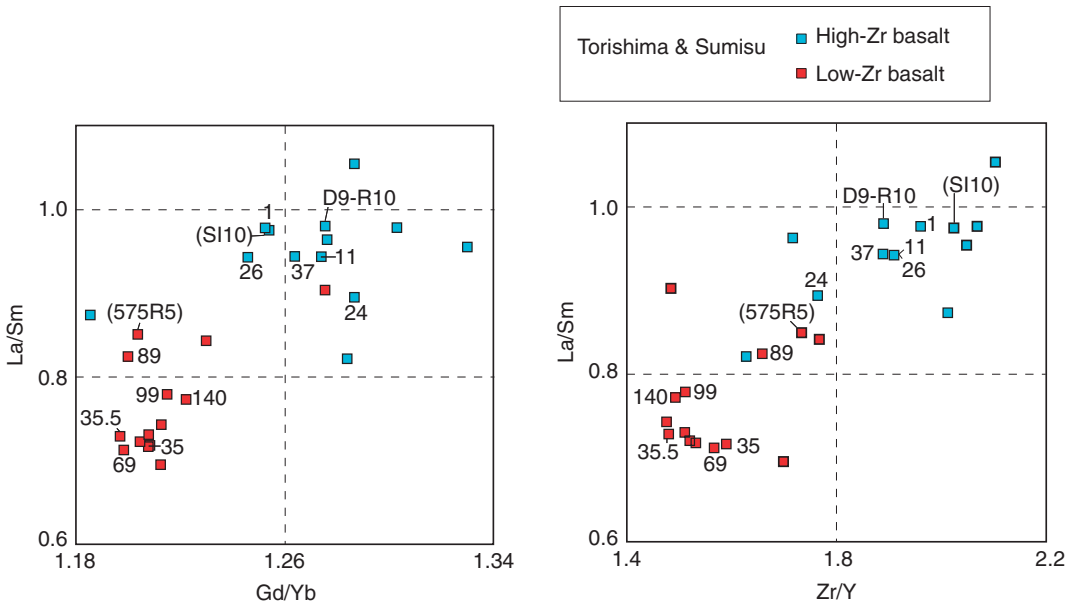

Fig. 12. La/Sm vs Gd/Yb and La/Sm vs Zr/Y for basalts from Torishima (this study) and Sumisu (Tamura *et al.*, 2005).

relative proportions of the mineral constituents that entered the melt. F^{L} is assumed to be 0·2 at the point of cpx-out, and thus the fraction of clinopyroxene in the source mantle is 0·127 according to the reaction, and that in the residue of the high-Zr basalt is between zero and 0·127.

Figure 13 shows the degree of melting for the high-Zr basalt (F^{H}) vs La/Sm in the low-Zr basalt assuming $F^{L}=0{\cdot}2$. F^{H} is determined using La/Sm values for pairs of high-Zr basalts and low-Zr basalts. The La/Sm ratios of the high-Zr basalts and their sample numbers are shown in the diagram. The La/Sm values of the low-Zr basalts range from 0·71 to 0·83. This variation could be caused by different degrees of partial melting within the low-Zr mantle source. However, we assumed that 20% partial melting produced each of the low-Zr basalt primary magmas. Thus, the degree of melting of the source of the high-Zr basalt increases with La/Sm in the paired low-Zr basalt. Table 3 shows the average from calculations made using 30 paired low-Zr and high-Zr basalts. The average F^{H} is 0·11 (Table 3). When 20% partial melting is assumed to produce the primary magmas of the low-Zr basalt, only ~11% melting is required to yield the high-Zr basalts (Table 3).

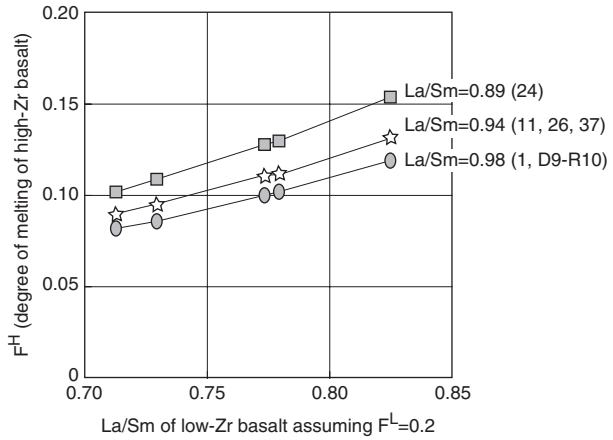

Fig. 13. Degree of melting of the source of high-Zr basalt (F^{H}) vs La/Sm in low-Zr basalt assuming $F^{L}=0{\cdot}2$. F^{H} is determined using La/Sm values for pairs of high-Zr basalt and low-Zr basalt. La/Sm of high-Zr basalts and their sample numbers are shown in the diagram. La/Sm values of low-Zr basalts range from 0·71 to 0·83. We assumed that 20% partial melting produced each of the low-Zr basalt primary magmas. The degree of melting of the high-Zr basalt increases with La/Sm in the paired low-Zr basalt, and the average F^{H} of 30 paired low-Zr and high-Zr basalts is 0·11 (Table 4).

FLUID-DERIVED COMPONENTS IN THE SOURCE OF THE TORISHIMA BASALTS

The positive correlations between La/Sm vs Gd/Yb and La/Sm vs Zr/Y (Fig. 12) at Sumisu and Torishima volcanoes and the calculations using La/Sm values (Fig. 13) suggest that the low-Zr basalts result from higher degrees of partial melting (~20%) than the high-Zr basalts (~11%). We therefore use Zr/Y as a proxy of the degree of melting of the mantle source. When we construct a diagram using incompatible element (A) on a Zr/Y vs A/Y plot, there should be a positive correlation if element A is more incompatible than Y in terms of partial melting of the source mantle. On the other hand, low-Zr basalts may have higher water contents than the high-Zr basalts under mantle conditions (Tamura *et al.*, 2005), where water is derived from the subducting lithosphere beneath the frontal volcanoes. Thus, any deviation from the partial melting trend will be the result of water, which can contain several specific elements, being added to the mantle source (e.g. Elliott, 2003).

Figure 14 shows the variation of Zr/Y vs A/Y (A = Rb, Ba, K_2O, Pb, and Sr) for the low-Zr and high-Zr basalts from Torishima volcano. K_2O/Y shows a positive correlation with Zr/Y, and the low-Zr basalts have lower K_2O/Y values than the high-Zr basalts. This is consistent with variations in the degree of melting in the source mantle. On the other hand, Pb/Y and Sr/Y, and to a lesser degree Ba/Y and Rb/Y, deviate from this melting trend,

Table 3: Average wt % of original and residual mineral phases, mantle/melt bulk partition coefficients and degree of melting (F) in the mantle source of the low-Zr and high-Zr basalts

	Olivine	Orthopyroxene	Clinopyroxene	D_{La}	D_{Sm}	F
Original mantle	61·8 ± 0·9	25·5 ± 0·9	12·7	–	–	0
Residual mantle (high-Zr)	71·3 ± 1·6	22·1 ± 0·9	6·6 ± 1·1	0·0049 ± 0·0008	0·036 ± 0·005	0·11 ± 0·02
Residual mantle (low-Zr)	81·6 ± 1·1	18·4 ± 1·1	0	0·00056 ± 0·00003	0·0041 ± 0·0002	0.2

Values represent average ± 1 SD from the mean of 30 low-Zr and high-Zr basalt pairs. Three assumptions are made; (1) original mantle has 12·7 wt % clinopyroxene; (2) residual mantle of low-Zr basalts contains no clinopyroxene; (3) degree of melting of low-Zr basalt source is 0·2. (See text for details.)

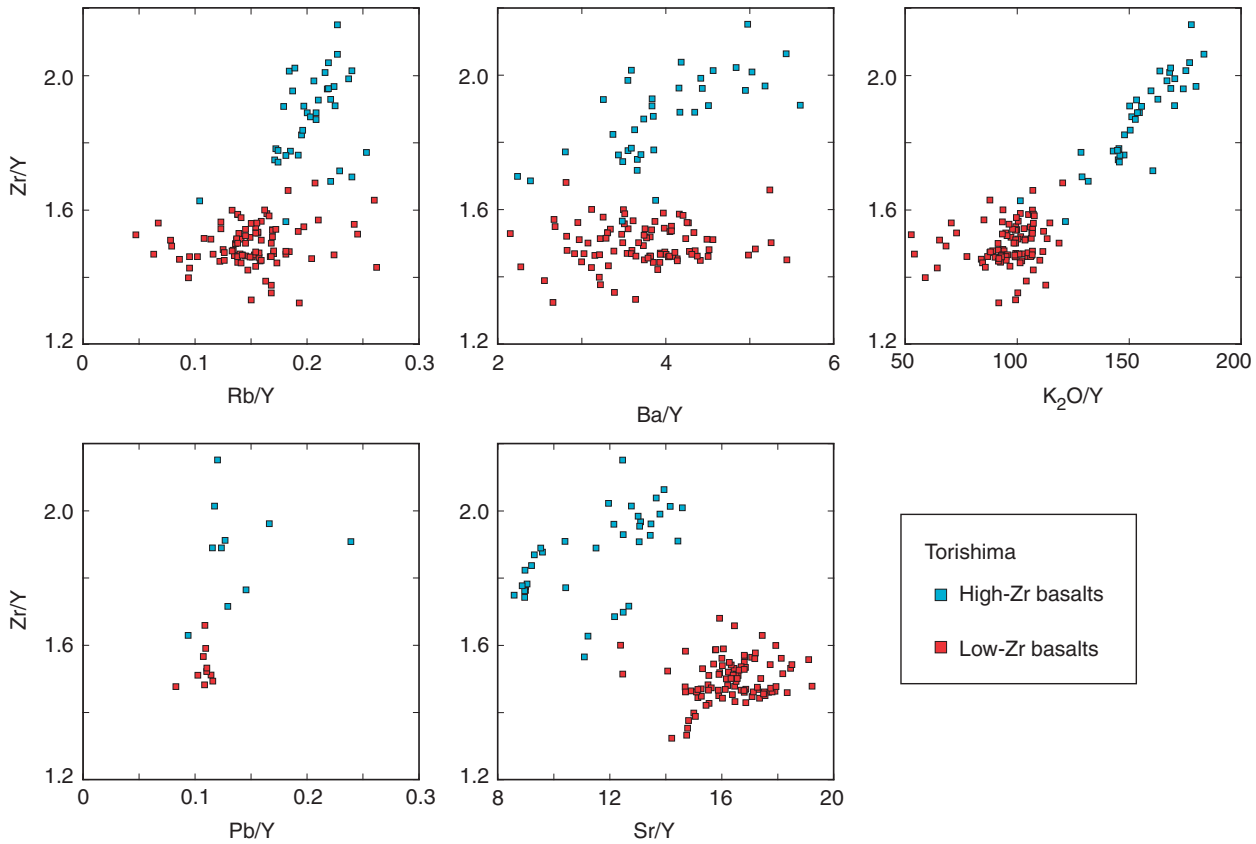

Fig. 14. Zr/Y vs Rb/Y, Ba/Y, K_2O/Y, Pb/Y and Sr/Y in Torishima high-Zr and low-Zr basalts.

showing relative enrichment of the low-Zr basalts in Pb and Sr compared with Y. Figure 15, presenting incompatible element data for representative samples of the low-Zr and high-Zr basalts, shows trends similar to those in Fig. 14. Elements assumed to be more incompatible than Sm, during partial melting of the source mantle and fractional crystallization of the parental basalt magmas, might be expected to form positive trends on these diagrams. Th and K form such trends, but Cs and Sr clearly do not. The lack of correlation for Cs and Sr could be explained by the addition of an aqueous fluid derived from the slab to the source mantle. The behaviour of Rb and Ba is intermediate between that of Th and K and Cs and Sr, suggesting that they are mildly immobile in the slab-derived aqueous fluids. Thus, we conclude that the REE, HFSE (Zr and Th), and K, and to a lesser degree Rb and Ba, follow degrees-of-melting expectations between high- and low-Zr basalts, but as shown in Figs 14 and 15, Cs, Pb and Sr do not. The latter elements are contained in arc-front slab-derived fluids. Rb and Ba exhibit variable behaviour in the low-Zr basalts, ranging from immobile, similar to K, to mildly enriched in some low-Zr basalts.

DISCUSSION

Effect of H_2O on phase stability of low- and high-Zr Torishima basalts

Basalts from Izu-Oshima, near the northern end of the Izu–Bonin arc, have compositions similar to the high-Zr basalts from Torishima, and also contain low-Ca pyroxene phenocrysts; the water content of these basalts was estimated to be <0·7% (Fujii *et al.*, 1988). In the Lesser Antilles volcanic arc, Macdonald *et al.* (2000) suggested that the relatively early appearance of orthopyroxene in the low-K suite of the Soufriere of St. Vincent, compared with St. Kitts and Montserrat, might indicate that the magmas were less hydrous, whereas its non-appearance in the C-series of Grenada is consistent with more hydrous crystallization. The appearance of orthopyroxene, however, may depend at least as much on the activity of silica as water.

We have no direct evidence for the H_2O content of the Torishima basalts, but phenocryst populations and experiments by other workers provide important information. There is apparent incompatibility of Al in both high- and low-Zr suites (Fig. 10a). Arguably, this could mean that the water content is high enough to suppress plagioclase

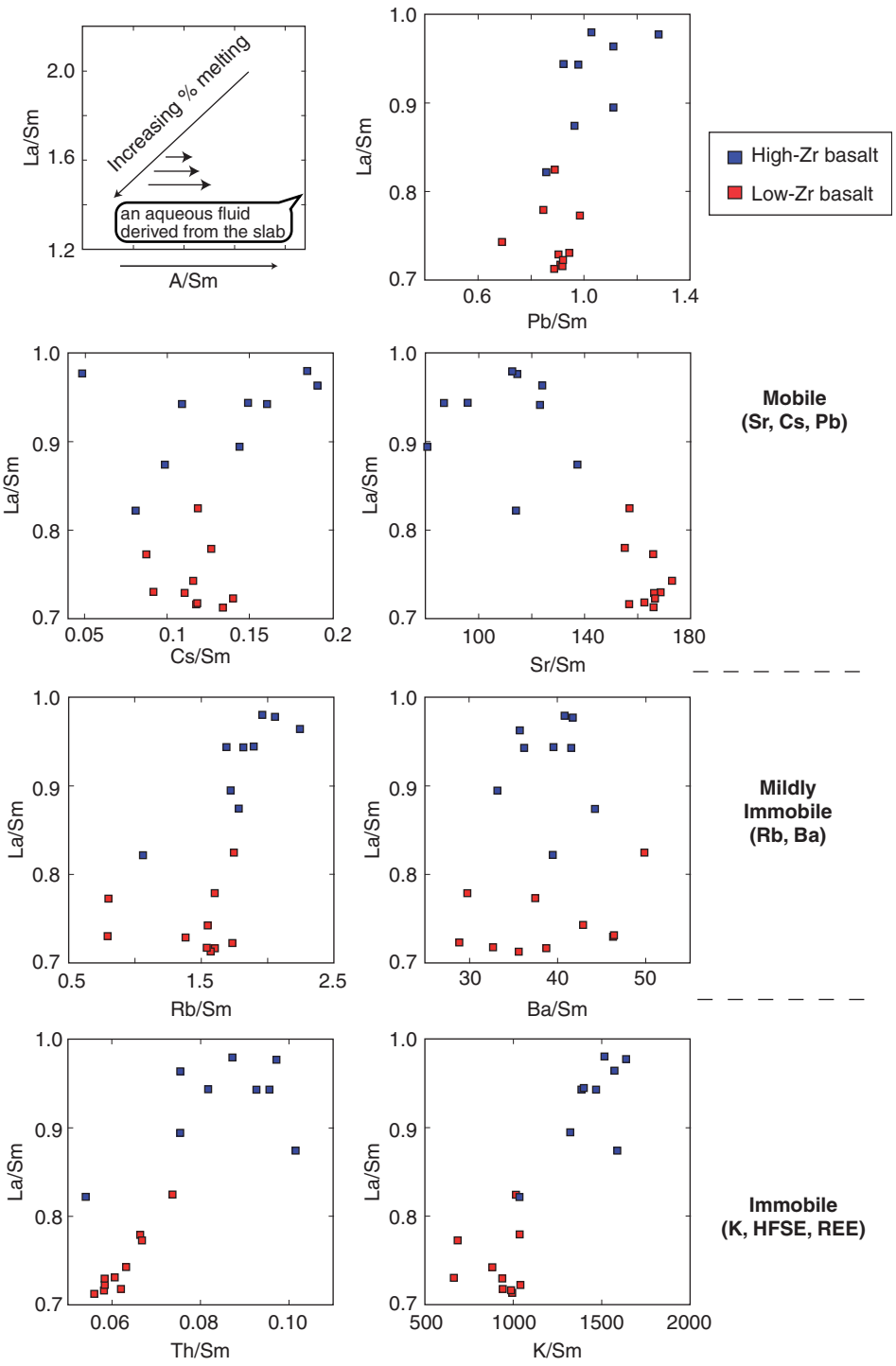

Fig. 15. La/Sm vs Pb/Sm, Cs/Sm, Sr/Sm, Rb/Sm, Ba/Sm, Th/Sm and K/Sm. La/Sm could be a measure of the degree of partial melting. Elements assumed to be more incompatible than Sm, during partial melting of source mantle and fractional crystallization of basalt magmas, might be expected to form positive trends in these diagrams. Th and K form such trends, but Cs and Sr clearly do not. The lack of correlation for Cs and Sr could be explained by the addition of an aqueous fluid derived from the slab to the source mantle. The behaviour of Rb and Ba is intermediate between that of Th and K and Cs and Sr, suggesting that they are mildly immobile in the aqueous fluid.

crystallization in both. Conversely, it could mean that plagioclase has accumulated in both, especially the high-Zr basalts. All low-Zr basalts in Sumisu and in Torishima contain olivine + clinopyroxene + plagioclase phenocrysts (except for the single differentiated sample shown in Fig. 6). In contrast, many Sumisu high-Zr basalts contain only olivine + plagioclase, and in Torishima, clinopyroxene appears as a phenocryst later than plagioclase in the crystallization sequence of the high-Zr basalts (Fig. 8). Nineteen of 37 high-Zr Torishima basalts contain orthopyroxene phenocrysts. Moreover, four Torishima high-Zr samples, having $FeO^*/MgO < 2{\cdot}0$, contain orthopyroxene phenocrysts, suggesting that orthopyroxene crystallizes earlier in the high-Zr basalts (Figs 6 and 7). Similar relationships have been discussed in part by Tamura *et al.* (2005).

Green (1982) showed experimentally that, under dry conditions in the 0–5 kbar pressure range, plagioclase is the major liquidus, or near-liquidus, phase in tholeiitic basalts and is subsequently joined by olivine and later by pyroxene. When 5% H_2O is added to a tholeiite, however, the appearance of plagioclase is markedly depressed, and pyroxene together with olivine become important near-liquidus phases from 2 to ~14 kbar (Green, 1982). Sisson & Grove (1993) demonstrated that at 2 kbar, with the addition of H_2O, the assemblage plagioclase + olivine + high-Ca pyroxene appears at high melt fractions, apparently close to the liquidus of high-alumina basalts. On the other hand, at low to moderate pressures, anhydrous high-alumina basalts crystallize plagioclase or olivine and plagioclase over extended temperature intervals before being joined by high-Ca pyroxene (Grove *et al.*, 1982; Baker & Eggler, 1983; Bartels *et al.*, 1991). Cotectic growth of augite is a likely consequence of an elevated magmatic water content that promotes expansion of the clinopyroxene phase volume. Kushiro (1969) showed that H_2O destabilizes low-Ca pyroxene in the system forsterite–diopside–silica. Sisson & Grove (1993) established that orthopyroxene crystallization from arc magmas is inhibited by high water contents; low-Ca pyroxene crystallizes in high-alumina basalts in 1 atm anhydrous experiments (Grove *et al.*, 1982) but does not in 2 kbar H_2O-saturated experiments (Sisson & Grove, 1993). These experimental results suggest that the phenocryst assemblage olivine + plagioclase crystallizes under dry conditions and thus the appearance of high-Ca pyroxene, together with olivine and plagioclase, requires a few per cent of water. Moreover, the early appearance of low-Ca pyroxene might be taken as an indication that the magmas were less hydrous.

Collectively, these findings qualitatively suggest that low-Zr basalt magmas containing phenocrystic olivine + clinopyroxene were hydrous, but that cpx-free or opx-bearing high-Zr magmas were dry.

Water and degrees of melting

Elliott *et al.* (1997) assumed that there is a fairly constant aqueous fluid flux along the entire Mariana arc, and they did not consider the degrees of melting of mantle sources. For example, in plots of fluid-immobile incompatible elements, the Mariana volcanic rocks display arrays that they inferred to reflect variable mixing of a sediment component with a depleted mantle wedge. Part of the variation, however, may have resulted from the effect of differing degrees of melting of a similar mantle wedge. Straub *et al.* (2004) separated low-K from very-low-K suites in tephra from ODP site 782A located ~120 km east of the Izu–Bonin Quaternary volcanic front. They concluded that the differences reflect the mass fraction of K-bearing fluid added to the wedge, based on the assumption that both suites resulted from an uniform (20%) degree of partial melting (batch melting) of the mantle source. In the South Sandwich Island arc, Pearce *et al.* (1995) concluded that the arc-melting event requires an average of 20% melting and suggested that some of the back-arc lavas in this area could have been derived by a smaller percentage of melting of a less depleted source. In the Aleutian arc, based on modal batch-melting models of lherzolite, Jicha *et al.* (2004) indicated that the compositions of the Roundhead and Shishaldin lavas require a 1·5–2·0% partial melt of a slightly modified MORB-source mantle, whereas Seguam lavas require a larger (1–5%) fluid addition to the mantle wedge and 22% partial melting of the fluid-enriched source. Luhr (1992) studied two contrasting Mexican volcanoes (Colima and Ceboruco) and concluded that the mantle wedge beneath Colima is more strongly affected by fluids rising from the slab, and this effect leads to higher percentages of partial melting (by a factor of 2·5) as compared with the Ceboruco source. A similar correlation between magmatic water content and degrees of partial melting was deduced by Stolper & Newman (1994) for basalts from the Mariana Trough, Kelley *et al.* (2006) for submarine basalts at several back-arc basins, and by Eiler *et al.* (2000), based chiefly on results from the Vanuatu arc. Tamura *et al.* (2005, and this study) have used data from Sumisu and Torishima to suggest that, within a single volcanic complex, the water content in the mantle source region can be heterogeneous, and this results in different degrees of partial melting of the source. These papers deal with basalts, but Kushiro (1990), Baker *et al.* (1994) and Tamura (1994) suggested that a heterogeneous distribution of H_2O in the mantle results in the production of a spectrum of mantle melts ranging from wet (calc-alkaline) to dry (tholeiitic).

In summary, from both regional and local points of view, a positive correlation might exist between the proportion of water in the source mantle and its degree of

melting; the maximum degree of melting of the arc source mantle is about 20%.

Aqueous fluids derived from the subducting slab beneath volcanic front volcanoes

Volcanic front magmatism along subduction zones is believed to be strongly influenced by a ubiquitous 'slab-fluid' component (e.g. Pearce, 1982; Hawkesworth *et al.*, 1993; Elliott, 2003). On the other hand, nearly H_2O-free magmas have been described along the Cascade arc and Izu–Bonin–Mariana arc (e.g. Nakano & Yamamoto, 1991; Sisson & Bronto, 1998; Kohut *et al.*, 2006). Tamura *et al.* (2005), furthermore, showed that both dry and wet primary basalts exist in the Sumisu magmatic system. The same two types of basalt are distributed widely on Torishima island. We can therefore compare wet and dry basalts from a single volcano, making it possible to identify the specific elements involved in fluid transport from the subducting slab. Figures 14–15 show that at Torishima Cs, Pb, and Sr were carried by these fluids, but K, Th and REE were not. Rb and Ba are mildly immobile. Interestingly, results from Torishima are consistent with the widely held views on the role of slab-fluid components in arc volcanoes (Elliott, 2003), based upon a comparison of basalt compositions in various arc settings with those erupted along mid-ocean ridges. Moreover, trace-element variations within the low-Zr basalts can be produced by the addition of fluid-derived components, so we can, therefore, estimate the proportion of a specific element derived from the fluids. For example, the Sr/Y of the low-Zr basalts ranges from 14 to 19 (Fig. 14) at similar Zr/Y values. If this variation is produced by the addition of Sr to the source mantle by fluids, 60–70% of the Sr in the low-Zr magmas could have been derived from the subducted slab (Fig. 14).

Based on isotopic and trace element data from the northern Izu–Bonin arc, Ishizuka *et al.* (2003) suggested the following: (1) about 35% of the Sr is derived from fluids from altered oceanic crust (AOC) at the volcanic front; (2) contributions from the slab are more significant for Pb, and the volcanic front requires 70–80% of the Pb from the slab-derived component; (3) Nd is almost exclusively mantle-derived in the volcanic front lavas, suggesting that the contribution of Nd from the slab-derived fluid is negligible. As shown in Figs 14 and 15, the wide and continuous range of variation in these fluid-mobile elements in the low-Zr basalts (at similar Zr/Y and La/Sm values) may reflect a range of fluid volumes added to the mantle wedge. Moreover, the positive trends displayed by the high-Zr basalts (Figs 14 and 15) are not always independent of the fluid additions, because relatively dry high-Zr magmas could contain some slab-derived fluids. Comparison of the results of Ishizuka *et al.* (2003) and this study may, therefore, not be appropriate, but at least the high mobility of Sr and Pb and the immobility of REE are mutually consistent.

Immobile potassium, LILE fractionation and the possible role of phengite

One new finding of this study is that K appears to be immobile in the slab below Torishima. Experimental studies on the stability of phengitic muscovite indicate that K-mica in the slab persists to depths much greater than the zone of melt generation beneath arcs (Domanik & Holloway, 1996; Schmidt, 1996). Schmidt (1996) and Schmidt & Poli (1998) showed that dehydration at low pressures is almost entirely associated with potassium-free phases, whereas at pressures above 30 kbar (~100 km depth) the role of phengite becomes increasingly important. Johnson & Plank (1999) performed dehydration and melting experiments on subducted sediments. They concluded that, with increasing temperature, Rb and K become less compatible in the subducted sediment, and the greatest change in their D values coincides with mica breakdown between 800 and 900°C at 2–3 GPa. This is consistent with our findings from the arc-front Torishima volcano, which show that wet (low-Zr) basalts do not contain excess K_2O compared with dry (high-Zr) basalts. Our study suggests the compatible behaviour of K in the downgoing slab beneath Torishima and Sumisu as compared with other incompatible elements (Figs 14 and 15). We suggest that this is the result of phengite stability at temperatures <800°C in the subducting slab below Torishima.

Experimentally determined partition coefficients for LILE between fluids and phengite at high pressures (2–4 GPa) and low temperatures (600–700°C) show that Cs strongly fractionates into the coexisting fluids (Melzer & Wunder, 2000; Green & Adam, 2003). Thus Rb/Cs and Ba/Cs ratios may provide discriminants for the micas involved (T. H. Green, personal communication, 2006). Figure 16 shows the variation of Ba/Cs vs Rb/Cs for Torishima basalts. The high-Zr basalts exhibit a positive correlation across a wider range of values than the low-Zr basalts, which plot in the lower portion of the high-Zr basalt field. The low-Zr basalts are enriched in the fluid-mobile element Cs (Fig. 15), and, moreover, they show LILE fractionation, resulting in lower Ba/Cs and Rb/Cs in the low-Zr basalts (Fig. 16). LILE variation and fractionation could have resulted from the addition of fluids derived from the subducting slab. The source mantle may have been variably enriched in Cs, reflected by the large variation in the high-Zr basalts. The narrow range shown by the low-Zr basalts may have arisen when the fluid-derived Cs dominated. It is also possible that some Ba and Rb may have also been added to the source mantle. Fluid addition to the mantle source will decrease Ba/Cs and Rb/Cs, because Cs does not partition into phengite and

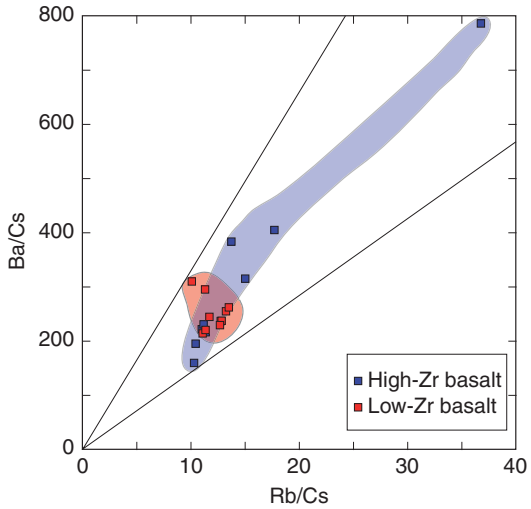

Fig. 16. Ba/Cs vs Rb/Cs for Torishima basalts.

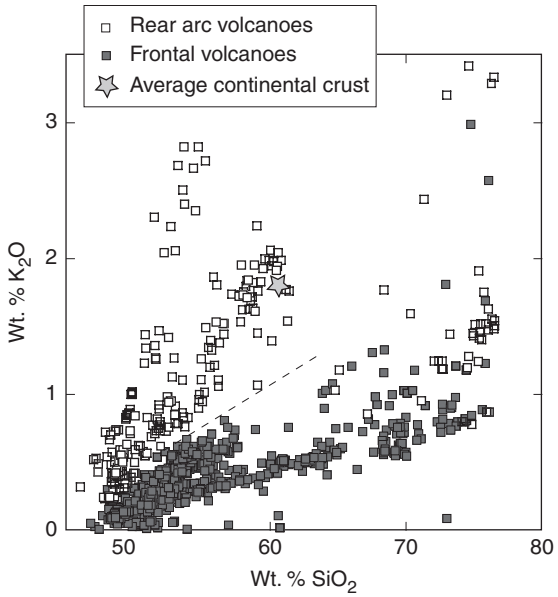

Fig. 17. K_2O vs SiO_2 (wt %) of lavas of the volcanic front (Oshima, Miyake-jima, Mikura-jima, Hachijojima, Aoga-shima, Myojin Knoll, Sumisu and Torishima), the rear arc (Kan'ei, Manji, Enpo, Genroku, Horeki) and average continental crust (Rudnick & Gao, 2003). Data are from Tamura & Tatsumi (2002) and references therein, Machida & Ishii (2003), Tamura *et al.* (2005), Tamura (unpublished data), Machida (unpublished data) and this study. For reasons of clarity, no field is shown for rift-type magmas (<3 Ma).

strongly partitions into the fluid, compared with Rb and Ba. We therefore suggest that H_2O-rich fluids originating from the subducting Pacific plate below the volcanic fronts of the Izu–Bonin arc may contain very little potassium. Instead, these fluids carry a large amount of Cs and, to a lesser degree, Rb and Ba, and cause fractionation of Ba/Cs and Rb/Cs, because K-bearing phengite is stable in the downgoing slab beneath the arc front. In contrast, potassium will be increasingly concentrated in the slab fluids as phengite breaks down when the subducted slab reaches depths of 100–300 km (Schmidt, 1996). We suggest that the increasing flux of potassium from the descending Pacific plate is responsible for the progressive enrichment of K in back-arc and cross-arc settings.

Structure and dynamics of the Izu–Bonin subduction zone

Geochemical observations

We have identified low-Zr and high-Zr basalts in both Sumisu and Torishima volcanoes, suggesting similarities in arc-front magma genesis in terms of water contents (dry and wet), degrees of melting (10–20%) and the major element chemistry of the source mantle (as interpreted from olivine compositions). On the other hand, arc-front and rear-arc volcanoes are dissimilar in terms of major element abundances, particularly K_2O and REE patterns (Gill, 1981; Tatsumi & Eggins, 1995). Such cross-arc asymmetry was recognized before the evolution of plate tectonic concepts (e.g. Kuno, 1959; Dickinson & Hatherton, 1967). Our findings suggest that K_2O and REE differences between the arc-front and rear-arc areas may be attributed to variation in the components derived from the downgoing slab.

Figure 17 shows the K_2O vs SiO_2 variation in lavas of the arc-front and rear-arc volcanoes of the northern part of the Izu–Bonin arc. A striking characteristic of orogenic andesites and associated rocks within many volcanic arcs of modest width is the consistent increase of their incompatible element concentrations, notably K_2O, away from the arc front (Gill, 1981). Basalts and andesites along the Izu–Bonin volcanic front contain significantly less K_2O than those from the rear of the arc (Fig. 17). Rocks from the frontal volcanoes form a low-K suite as defined by Gill's (1981) criterion, but the rear-arc lavas are medium- and high-K. This across-arc variation is almost the same as found in the NE Japan arc (e.g. Tamura, 2003; Kimura & Yoshida, 2006). Basalt and andesite magmas at the front of the Izu–Bonin arc are so depleted in K_2O that they are dissimilar to the 'average continental crust' of Rudnick & Gao (2003).

Figure 18 shows a C1 chondrite-normalized REE plot for the Izu–Bonin basalts and andesites. All basalts from arc-front volcanoes are strongly depleted in the more incompatible LREE compared with the MREE and HREE. In contrast, basalts and andesites from rear-arc sites are enriched in the LREE and MREE compared with the HREE (Fig. 18). Thus, rear-arc compositions are closer approximations to the average continental crust of Rudnick & Gao (2003).

Figure 19 shows along-arc Sr–Nd–Pb isotopic variations in lavas from frontal volcanoes, rear-arc volcanoes,

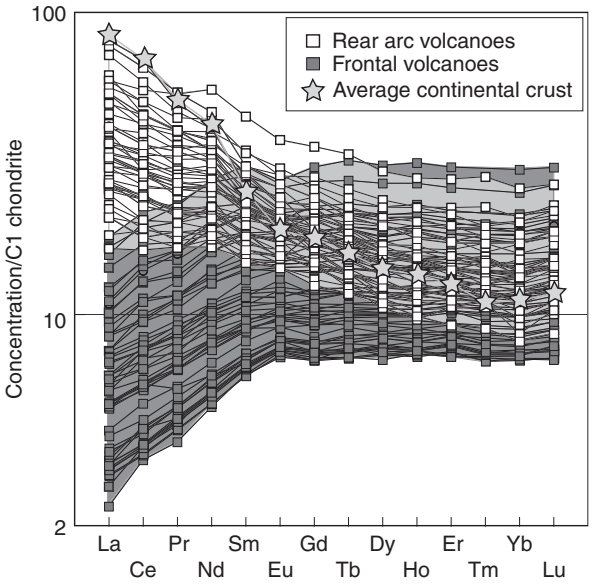

Fig. 18. Chondrite-normalized rare earth element (REE) abundances in the volcanic front and the rear-arc basalts and andesites and average continental crust (Rudnick & Gao, 2003). Data for the volcanic front (Oshima, Miyake-jima, Hachijojima, Aoga-shima, Sumisu, Torishima) from Taylor & Nesbitt (1998), Tamura *et al.* (2005) and this study. Rear-arc data (Kan'ei, Manji, Enpo, Genroku, Horeki) from Hochstaedter *et al.* (2001), Ishizuka *et al.* (2003), Machida & Ishii (2003) and Ishizuka (unpublished data). Rear-arc patterns deviate only slightly from average continental crust.

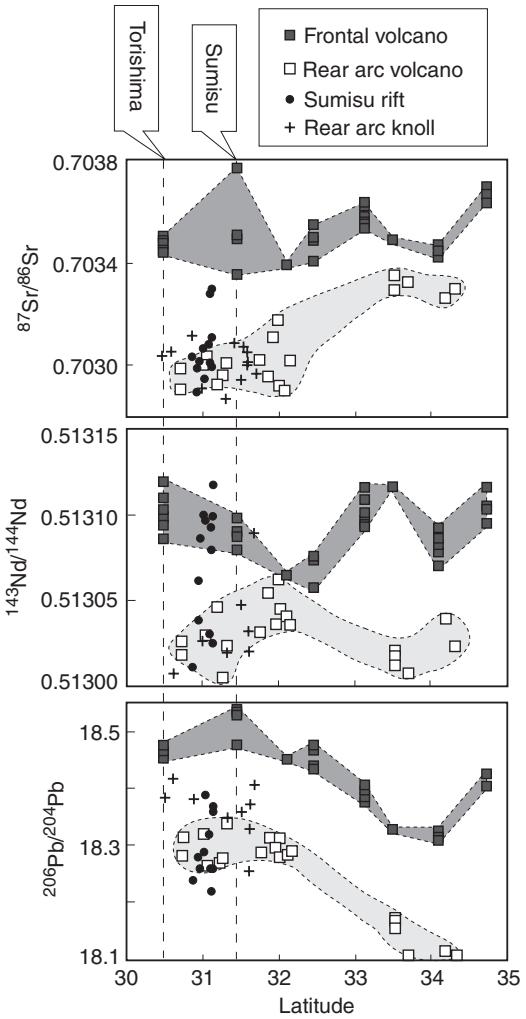

Fig. 19. Along-arc Sr–Nd–Pb isotopic variations in lavas from frontal arc volcanoes, Sumisu Rift, rear-arc knoll and rear-arc volcanoes. Data are from Taylor & Nesbitt (1998) (Quaternary frontal volcanoes), Tamura *et al.* (2005) (Sumisu), Hochstaedter *et al.* (1990) (Sumisu Rift), and Ishizuka *et al.* (2003) (Quaternary frontal volcanoes, rear-arc volcanoes and rear-arc knolls).

the Sumisu Rift and rear-arc knolls, based mostly on the data of Taylor & Nesbitt (1988), Ishizuka *et al.* (2003) and Sumisu data from Tamura *et al.* (2005). There may be some differences between Sumisu and Torishima, with Torishima having higher Nd but lower Pb isotope ratios (more depleted in both). However, the differences are much smaller than those between frontal volcanoes and rear-arc volcanoes (Fig. 19). Basalts and andesites of the rear-arc volcanoes contain less radiogenic Sr, Nd, and Pb isotopes compared with the volcanic front (Hochstaedter *et al.*, 2000; Ishizuka *et al.*, 2003). On the other hand, at both Sumisu and Torishima, there is no isotopic difference between the two suites (low- and high-Zr) of basalts, which may be a problem for the idea that the other differences are caused by more slab fluid in the low-Zr suites at both localities. Each frontal- and rear-arc volcano has a limited range of isotopic compositions compared with those from the Sumisu Rift. Moreover, the along-arc variations are coherent between the volcanic front and the rear arc (Ishizuka *et al.*, 2003).

A possible model

The diapir model of Tamura (2003) and Tamura *et al.* (2005) provides a possible explanation. Figure 20 shows a cross-arc section along the axis of a mantle-wedge hot finger (Tamura *et al.*, 2002), modified from Tamura (2003) and Tamura *et al.* (2005). Enriched MORB (E-MORB) source mantle, represented by the Sumisu Rift source (Hochstaedter *et al.*, 1990), is replenished by mantle materials [normal MORB (N-MORB) source] carried by conveyor-like convection (Tamura *et al.*, 2005). Mantle diapirs, the interpreted source mantle of individual arc volcanoes, are produced just above the slab and consist of mixtures of hot-finger and surrounding mantle-wedge materials (Tamura, 2003). Mantle diapirs below the volcanic front contain mostly depleted mantle with a greater slab fluid component. We conclude that the limit of phengite stability in subducted sediments is deeper than the depth of the slab just below the low-K frontal volcanoes (e.g. Sumisu and Torishima). As the sediments are carried deeper with subducting lithosphere, at some

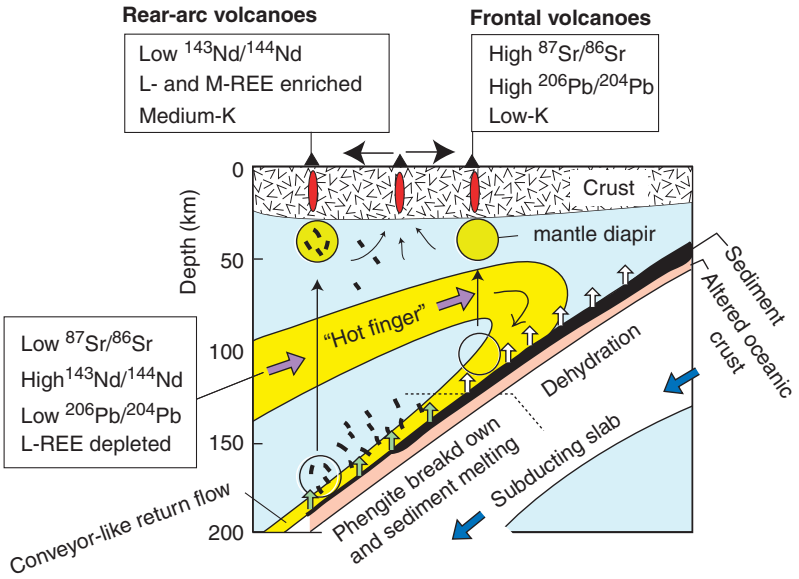

Fig. 20. Section along the axis of a mantle wedge 'hot finger', modified from Tamura (2003), Tamura *et al.* (2005) and Ishizuka *et al.* (2006). A 'hot finger' is the result of asthenospheric flow and upwelling within the mantle wedge (Tamura *et al.*, 2002). MORB-source mantle in the ambient mantle wedge (Hochstaedter *et al.*, 1990) is replenished by conveyor-like convection within a hot finger, which consists of mantle materials depleted in mantle-derived fluid-immobile elements and having low $^{87}Sr/^{86}Sr$, high $^{143}Nd/^{144}Nd$ and low $^{206}Pb/^{204}Pb$. Magmas at the volcanic front are rich in the fluid-mobile recycled slab components that modify the mantle diapir, resulting in high $^{87}Sr/^{86}Sr$ and $^{206}Pb/^{204}Pb$. Magmas at the rear-arc volcanoes are rich in low $^{143}Nd/^{144}Nd$ sediment melt components (LREE, MREE and K enriched), which were derived from the subducting slab. A major interpretation of this study is that K is immobile in the slab below the frontal volcanoes of Sumisu and Torishima, where phengite is stable, but K is highly mobile in deeper, back-are environments, where phengite breaks down. Phengite thus plays an important role in arc magma genesis.

point they begin to melt, and phengite begins to break down and is eventually consumed. Johnson & Plank (1999) showed that, as the sediment solidus is crossed, phengite is the first hydrous phase to be consumed. Thus, K_2O differences between the arc-front and back-arc may be attributed to variations in components derived from the slab. Within the eastern, shallower part of the slab, phengite is stable, and K is, therefore, immobile. Further west, and at greater depth, phengite breaks down and K-rich fluids or melts are added to the mantle source (Fig. 20).

Another possible scenario is that magma is first extracted in the western part of the finger and is then extracted a second time as the depleted mantle moves eastward and is again fluxed by fluid from the slab (Hochstaedter *et al.*, 2000, 2001). This model, however, fails to explain the similarly depleted olivine compositions in both the front- and rear-arc regions, which is not consistent with eastward mantle source depletion at depth. Some olivines from a rear-arc volcano have $Fo_{>92}$, with ~0·4 wt % NiO, suggesting a magnesian, depleted mantle source resulting from higher degrees of melting (Tamura *et al.*, in preparation).

Ishizuka *et al.* (2003) suggested that a strong correlation between Sr isotope composition and fluid-mobile element enrichment in volcanic front lavas implies a significant contribution of slab-derived fluid to the volcanic front magma source. This results in higher Sr-isotope ratios at frontal-arc volcanoes compared with those at rear-arc and rift-related sites (Fig. 20). They further suggested that high delta 7/4 Pb and low $^{143}Nd/^{144}Nd$ associated with high Th/Ce imply that subducted sediment is an important component in the back-arc. Phengite breaks down at about 50°C above the sediment solidus (Johnson & Plank, 1999); thus the sediment component and K_2O contents of magmas should be closely correlated. Actually they are correlated, as shown in Fig. 20. Ishizuka *et al.* (2006) further suggested temporal and spatial variations in the Izu–Bonin arc magmatism and concluded that the angle of subducting Pacific Plate became steeper with time. Figure 20 is based on Ishizuka *et al.* (2006, fig. 15).

Elliott *et al.* (1997) presented two physical models to account for the key geochemical features observed in arc-front Mariana lavas, one involving sediment melting below the arc front and the other calling for sediment melting below the back-arc and the migration of this melt to sites below the arc front. Because both arc-front and back-arc volcanoes are present in the Izu–Bonin arc, we were able to recognize the separate processes of fluid dehydration and sediment melting in volcanoes across the arc. We therefore prefer the second model of Elliott *et al.* (1997), and Fig. 20 is a modification of this.

CONCLUSIONS

The arc-front Izu–Bonin volcanoes of Sumisu and Torishima contain basalts originating from both wet and dry parental basalt magmas (low- and high-Zr basalts, respectively). These magmas result from different degrees of melting of the same source mantle (~20% and ~10% for wet and dry basalt magmas, respectively), and their Zr and K_2O contents have negative correlations with the degree of melting.

Assuming that wet basalts contain higher percentages of slab-derived components, comparison of these two types of basalts at Torishima makes it possible to identify the specific elements involved in fluid transport from the subducting slab. We conclude that Cs, U, Pb and Sr are variably and selectively concentrated in the slab-derived fluids below the arc-front Torishima volcano, whereas K, HFSE and REE are not. Rb and Ba exhibit variable behaviour in the low-Zr basalts, ranging from immobile, similar to K, to mildly enriched in some low-Zr basalts. Moreover, LILE fractionation in the slab-derived fluids is illustrated by Rb/Cs and Ba/Cs variations. Phengite is probably stable in the shallower slab underlying the arc front, thus accounting for the paucity of potassium and LILE fractionation in arc-front magmatic systems. Cross-arc variations may therefore be related to the transient stability of phengite in the downgoing slab.

ACKNOWLEDGEMENTS

Dredge samples used in this study were collected during a JAMSTEC cruise in December 2002 (KR02-16). We are indebted to Captain O. Yukawa of R.V. *Kairei* and the crew. We also thank James Gill, Stephen Parman and Tim Elliott for careful and insightful reviews, and Richard Fiske, Alex Nichols and John Gamble for editorial help. Part of this research was supported by a Grant-in-Aid for Scientific Research (B) (17340165) to Y.T. from the Japan Society for the Promotion of Science (JSPS). Field studies on Torishima island by Y.T. and K.T. were supported by Ikuo Kushiro, Yoshiyuki Tatsumi and IFREE Research Promotion Office. Marjorie Wilson greatly assisted in improving the style and content of the final product.

SUPPLEMENTARY DATA

Supplementary data for this paper are available at *Journal of Petrology* online.

REFERENCES

Baker, D. R. & Eggler, D. H. (1983). Fractionation paths of Atka (Aleutians) high-alumina basalts: constraints from phase relations. *Journal of Volcanology and Geothermal Research* **18**, 387–404.

Baker, M. B., Grove, T. L. & Price, R. (1994). Primitive basalts and andesites from the Mt. Shasta region, N. California: products of varying melt fraction and water content. *Contributions to Mineralogy and Petrology* **118**, 111–129.

Bartels, K. S., Kinzler, R. J. & Grove, T. L. (1991). High-pressure phase relations of primitive high-alumina basalt from Medicine Lake volcano, northern California. *Contributions to Mineralogy and Petrology* **108**, 253–270.

Chang, Q., Shibata, T., Shinotsuka, K., Yoshikawa, M. & Tatsumi, Y. (2003). Precise determination of trace elements in geological standard rocks using inductively coupled plasma mass spectrometry. *Frontier Research on Earth Evolution (IFREE Report for 2001–2002)* **1**, 357–362.

Dickinson, W. R. & Hatherton, T. (1967). Andesite volcanism and seismicity around the Pacific. *Science* **157**, 801–803.

Domanik, K. J. & Holloway, J. R. (1996). The stability and composition of phengitic muscovite and associated phases from 5·5 to 11 GPa: Implications for deeply subducted sediments. *Geochimica et Cosmochimica Acta* **60**, 4133–4150.

Eiler, J. M., Crawford, A., Elliott, T., Farley, K. A., Valley, J. W. & Stolper, E. M. (2000). Oxygen isotope geochemistry of oceanic-arc lavas. *Journal of Petrology* **41**, 229–256.

Elliott, T. (2003). Tracers of the slab. In: Eiler, J. (ed.) *Inside the Subduction Factory. Geophysical Monograph, American Geophysical Union* **138**, 23–45.

Elliott, T., Plank, T., Zindler, A., White, W. & Bourdon, B. (1997). Element transport from slab to volcanic front at the Mariana arc. *Journal of Geophysical Research* **102**, 14991–15019.

Fujii, T., Aramaki, S., Kaneko, T., Ozawa, K., Kawanabe, Y. & Fukuoka, T. (1988). Petrology of the lavas and ejecta of the November, 1986 eruption of Izu-Oshima volcano. *Bulletin of the Volcanological Society of Japan* **33**, S234–S254 (in Japanese with English abstract and figure captions).

Gaetani, G. A. & Grove, T. L. (1998). The influence of water on melting of mantle peridotite. *Contributions to Mineralogy and Petrology* **131**, 323–346.

Gaetani, G. A., Kent, A. J. R., Grove, T. L., Hutcheon, I. D. & Stolper, E. M. (2003). Mineral/melt partitioning of trace elements during hydrous peridotite partial melting. *Contributions to Mineralogy and Petrology* **145**, 391–405.

Gill, J. (1981). *Orogenic Andesites and Slab Tectonics*. Berlin: Springer.

Gill, J. B., Hiscott, R. N., Vidal, & Ph., (1994). Turbidite geochemistry and evolution of the Izu–Bonin arc and continents. *Lithos* **33**, 135–168.

Green, T. H. (1982). Anatexis of mafic crust and high pressure crystallization of andesite. In: Thorpe, R. S. (ed.) *Andesites*. New York: John Wiley, pp. 465–487.

Green, T. H. & Adam, J. (2003). Experimentally-determined trace element characteristics of aqueous fluid from partially dehydrated mafic oceanic crust at 3·0 GPa, 650–700°C. *European Journal of Mineralogy* **15**, 815–830.

Grove, T. L., Gerlach, D. C. & Sando, T. W. (1982). Origin of calc-alkaline series lavas at Medicine Lake volcano by fractionation, assimilation and mixing. *Contributions to Mineralogy and Petrology* **80**, 160–182.

Hawkesworth, C. J., Gallagher, K., Hergt, J. M. & McDermott, T. (1993). Mantle and slab contribution in arc magmas. *Annual Review of Earth and Planetary Sciences* **21**, 175–204.

Hirschmann, M. M., Asimow, P. D., Ghiorso, M. S. & Stolper, E. M. (1999). Calculation of peridotite melting from thermodynamic models of minerals and melts. III. Controls on isobaric melt production and the effect of water on melt production. *Journal of Petrology* **40**, 831–851.

Hochstaedter, A. G., Gill, J. B. & Morris, J. D. (1990). Volcanism in the Sumisu Rift, II. Subduction and non-subduction related components. *Earth and Planetary Science Letters* **100**, 195–209.

Hochstaedter, A. G., Gill, J. B., Taylor, B., Ishizuka, O., Yuasa, M. & Morita, S. (2000). Across-arc geochemical trends in the Izu–Bonin arc: Constraints on source composition and mantle melting. *Journal of Geophysical Research* **105**, 495–512.

Hochstaedter, A., Gill, J., Peters, R., Broughton, P. & Holden, P. (2001). Across-arc geochemical trends in the Izu–Bonin arc: Contributions from the subducting slab. *Geochemistry, Geophysics, Geosystems* **2**, paper number 2000GC000105.

Imai, N., Terashima, S., Itoh, S. & Ando, A. (1995). 1994 compilation values for GSJ reference samples, Igneous rock series. *Geochemical Journal* **29**, 91–95.

Ishizuka, O., Taylor, R. N., Milton, J. A. & Nesbitt, R. W. (2003). Fluid–mantle interaction in an intra-oceanic arc: constraints from high-precision Pb isotopes. *Earth and Planetary Science Letters* **211**, 221–236.

Ishizuka, O., Taylor, R. N., Milton, J. A., Nesbitt, R. W., Yuasa, M. & Sakamoto, I. (2006). Variation in the mantle sources of the northern Izu arc with time and space—constraints from high-precision Pb isotopes. *Journal of Volcanology and Geothermal Research* **156**, 266–290.

Jicha, B. R., Singer, B. S., Brophy, J. G., Fournelle, J. H., Johnson, C. M., Beard, B. L., Lapen, T. J. & Mahlen, N. J. (2004). Variable impact of the subducted slab on Aleutian island arc magma sources: evidence from Sr, Nd, Pb, and Hf isotopes and trace element abundances. *Journal of Petrology* **45**, 1845–1875.

Johnson, M. C. & Plank, T. (1999). Dehydration and melting experiments constrain the fate of subducted sediments. *Geochemistry, Geophysics, Geosystems* **1**, paper number 1999GC000014.

Kelley, K. A., Plank, T., Grove, T. L., Stolper, E. M., Newman, S. & Hauri, E. (2006). Mantle melting as a function of water content beneath back-arc basins. *Journal of Geophysical Research* **111**, B09208, doi:10.1029/2005JB003732.

Kimura, J. I. & Yoshida, T. (2006). Contributions of slab fluid, mantle wedge and crust to the origin of Quaternary lavas in the NE Japan arc. *Journal of Petrology* **47**, 2185–2232.

Kohut, E. J., Stern, R. J., Kent, A. J. R., Nielsen, R. L., Bloomer, S. H. & Leybourne, M. (2006). Evidence for adiabatic decompression melting in the Southern Mariana Arc from high-Mg lavas and melt inclusions. *Contributions to Mineralogy and Petrology* **152**, 201–211.

Kuno, H. (1959). Origin of Cenozoic petrographic provinces of Japan and surrounding areas. *Bulletin of Volcanology* **32**, 141–176.

Kuno, H. (1960). High-alumina basalt. *Journal of Petrology* **1**, 121–145.

Kuno, H. (1966). Lateral variation of basalt magma type across continental margins and island arcs. *Bulletin Volcanologique* **29**, 195–222.

Kushiro, I. (1969). The system forsterite–diopside–silica with and without water at high pressures. *American Journal of Science* **267A**, 269–294.

Kushiro, I. (1990). Partial melting of mantle wedge and evolution of island arc crust. *Journal of Geophysical Research* **95**, 15929–15939.

Kushiro, I. (1994). Recent experimental studies on partial melting of mantle peridotites at high pressures using diamond aggregates. *Journal of Geological Society of Japan* **100**, 103–110.

Luhr, J. F. (1992). Slab-derived fluids and partial melting in subduction zones: insights from two contrasting Mexican volcanoes (Colima and Ceboruco). *Journal of Volcanology and Geothermal Research* **54**, 1–18.

Maaløe, S. (1994). Estimation of the degree of partial melting using concentration ratios. *Geochimica et Cosmochimica Acta* **58**, 2519–2525.

Maaløe, S. & Pedersen, R. B. (2003). Two methods for estimating the degree of melting and trace element concentrations in the sources of primary magmas. *Chemical Geology* **193**, 155–166.

Macdonald, R., Hawkesworth, C. J. & Heath, E. (2000). The Lesser Antilles volcanic chain: a study in arc magmatism. *Earth-Science Reviews* **49**, 1–76.

Machida, S. & Ishii, T. (2003). Backarc volcanism along the en echelon seamounts: the Empo seamount chain in the northern Izu–Ogasawara arc. *Geochemistry, Geophysics, Geosystems* **4**, 9006, doi:10.1029/2003GC000554.

McDade, P., Blundy, J. D. & Wood, B. J. (2003a). Trace element partitioning between mantle wedge peridotite and hydrous MgO-rich melt. *American Mineralogist* **88**, 1825–1831.

McDade, P., Blundy, J. D. & Wood, B. J. (2003b). Trace element partitioning on the Tinaquillo lherzolite solidus at 1·5 GPa. *Physics of the Earth and Planetary Interiors* **139**, 129–147.

Melzer, S. & Wunder, B. (2000). Island-arc basalt alkali ratios: Constraints from phengite–fluid partitioning experiments. *Geology* **28**, 583–586.

Nakano, S. & Yamamoto, T. (1991). Chemical variations of magmas at Izu-Oshima volcano, Japan: plagioclase-controlled and differentiated magmas. *Bulletin of Volcanology* **53**, 112–120.

Pearce, J. A. (1982). Trace element characteristics of lavas from destructive plate boundaries. In: Thorpe, R. S. (ed.) *Andesites*. New York: John Wiley, pp. 525–548.

Pearce, J. A., Baker, P. E., Harvey, P. K. & Luff, I. W. (1995). Geochemical evidence for subduction fluxes, mantle melting and fractional crystallization beneath the South Sandwich Island arc. *Journal of Petrology* **36**, 1073–1109.

Rudnick, R.L. & Gao, S. (2003). The Composition of the Continental Crust. In Rudnick, R.L. (ed.) *The Crust* Vol. 3, Treatise on Geochemistry (eds. H.D. Holland and K.K. Turekian), Elsevier-Pergamon, Oxford, pp. 1–64.

Sakuyama, M. & Nesbitt, R. W. (1986). Geochemistry of the Quaternary volcanic rocks of the Northeast Japan arc. *Journal of Volcanology and Geothermal Research* **29**, 413–450.

Schmidt, M. W. (1996). Experimental constraints on recycling of potassium from subducted oceanic crust. *Science* **272**, 1927–1930.

Schmidt, M. W. & Poli, S. (1998). Experimentally based water budgets for dehydrating slabs and consequences for arc magma generation. *Earth and Planetary Science Letters* **163**, 361–379.

Shukuno, H., Tamura, Y., Tani, K., Chang, Q., Suzuki, T. & Fiske, R. S. (2006). Origin of silicic magmas and the compositional gap at Sumisu submarine caldera, Izu–Bonin arc, Japan. *Journal of Volcanology and Geothermal Research* **156**, 187–216.

Sisson, T. W. & Bronto, S. (1998). Evidence for pressure-release melting beneath magmatic arcs from basalt at Galunggung, Indonesia. *Nature* **391**, 883–886.

Sisson, T. W. & Grove, T. L. (1993). Experimental investigations of the role of H_2O in calc-alkaline differentiation and subduction zone magmatism. *Contributions to Mineralogy and Petrology* **113**, 143–166.

Stolper, E. & Newman, S. (1994). The role of water in the petrogenesis of Mariana Trough magmas. *Earth and Planetary Science Letters* **121**, 293–325.

Straub, S. M., Layne, G. D., Schmidt, A. & Langmuir, C. H. (2004). Volcanic glasses at the Izu arc volcanic front: New perspectives on fluid and sediment melt recycling in subduction zones. *Geochemistry, Geophysics, Geosystems* **5**, doi:10.1029/2002GC000408.

Sun, S.-S. & McDonough, W. F.Chemical and isotopic systematics of oceanic basalts: implications for mantle composition and processes. In: Saunders, A. D. & Norry, M. J. (eds) *Magmatism in the Ocean*

Basins London: Special Publications, Geological Society **42**, 313–345.

Tamura, Y. (1994). Genesis of island arc magmas by mantle-derived bimodal magmatism: evidence from the Shirahama Group, Japan. *Journal of Petrology* **35**, 619–645.

Tamura, Y., Yuhara, M. & Ishii, T. (2000). Primary arc basalts from Daisen volcano, Japan: equilibrium crystal fractionation versus disequilibrium fractionation during supercooling. *Journal of Petrology* **41**, 431–448.

Tamura, Y. & Tatsumi, Y. (2002). Remelting of an andesitic crust as a possible origin for rhyolitic magma in oceanic arcs: an lexample from the Izu–Bonin arc. *Journal of Petrology* **43**, 1029–1047.

Tamura, Y., Tatsumi, Y., Zhao, D., Kido, Y. & Shukuno, H. (2002). Hot fingers in the mantle wedge: new insights into magma genesis in subduction zones. *Earth and Planetary Science Letters* **197**, 107–118.

Tamura, Y. (2003). Some geochemical constraints on hot fingers in the mantle wedge: evidence from NE Japan. In: Larter, R. D. & Leat, P. T. (eds) *Intra-Oceanic Subduction Systems: Tectonic and Magmatic Processes. Special Publications, Geological Society, London* **219**, 221–237.

Tamura, Y., Tani, K., Ishizuka, O., Chang, Q., Shukuno, H. & Fiske, R. S. (2005). Are arc basalts dry, wet, or both? Evidence from the Sumisu caldera volcano, Izu–Bonin arc, Japan. *Journal of Petrology* **46**, 1769–1803.

Tani, K., Fiske, R. S., Tamura, Y., Kido, Y., Naka, J., Shukuno, H. & Takeuchi, L. (2007). Sumisu volcano, Izu–Bonin arc, Japan: site of a silicic caldera-forming eruption from a small open-ocean island. *Bulletin of Volcanology*, doi:10.1007/s004455-007-0153-2.

Tatsumi, Y. & Eggins, S. M. (1995). *Subduction Zone Magmatism*. Cambridge, MA: Blackwell.

Taylor, B. (1992). Rifting and the volcanic–tectonic evolution of the Izu–Bonin–Mariana arc. In: Taylor, B. & Fujioka, K. *et al*. (eds) *Proceeding of the Ocean Drilling Program, Scientific Results, 126*. College Station, TX: Ocean Drilling Program, pp. 627–651.

Taylor, R. N. & Nesbitt, R. W. (1998). Isotopic characteristics of subduction fluids in an intra-oceanic setting, Izu–Bonin arc, Japan. *Earth and Planetary Science Letters* **164**, 79–98.